The 2006 Eruption of Augustine Volcano, Alaska
Power, J.A., Coombs, M.L., and Freymueller, J.T., editors
U.S. Geological Survey Professional Paper 1769

Chapter 20

Integrated Satellite Observations of the 2006 Eruption of Augustine Volcano

By John E. Bailey[1,2], Kenneson G. Dean[1], Jonathan Dehn[1], and Peter W. Webley[1]

Abstract

Satellite observations played an important role in monitoring the 2006 eruption of Augustine Volcano. It represented the first opportunity for observers to use, in an operational setting, new Web-based tools and techniques developed by the Alaska Volcano Observatory remote sensing group. The "Okmok Algorithm" was used to analyze thermal infrared satellite data and highlight changes in the style and phases of activity. Temperature measurements were used to estimate ash cloud heights, which compared favorably to radar and ground-based observations, although larger discrepancies were seen when compared to pilot reports. Brightness temperature difference techniques were used to locate and track the 14 ash clouds produced during the explosive phase of the eruption. Stacking of these analyses allowed the creation of composite maps showing the distribution of airborne ash. The data from these maps were further combined with information from local reports and samples of ashfall to create a prototype of a concentration map that could be used to assess the potential hazard an eruption represents to aircraft, infrastructure and human health.

Introduction

The Alaska Volcano Observatory (AVO) monitors volcanoes in Alaska using a combination of geophysical, geological, and remote sensing data. AVO is responsible for providing both government authorities and the general public with information concerning hazards related to volcanoes that are currently in or showing increased potential for eruption. In particular, the detection of volcanic ash plumes and clouds is critical because of the potential of ash to damage machinery, adversely affect human health, and disrupt transportation infrastructure. AVO issues reports in conjunction with the National Weather Service (NWS) through the Anchorage Volcanic Ash Advisory Center (VAAC) and Federal Aviation Administration (FAA) to alert aircraft to the presence of potentially hazardous volcanic ash clouds.

The need for a volcanic hazards monitoring program in Alaska was highlighted during the December 1989 eruption of Redoubt Volcano (Dean and others, 1994; Miller and Chouet, 1994), when a Boeing 747 flew into the Redoubt ash cloud, causing all four engines to fail (Casadevall, 1994). A catastrophic loss of life was averted by the pilot restarting engines less than 2 minutes before impact. Damage to the aircraft was estimated at $80 million. Using a combination of satellite datasets and analysis methods, AVO is now able to track ash clouds similar to those from Redoubt and predict their probable dispersion patterns (Webley and others, this volume). In addition, other techniques using satellite data aid evaluation of precursory activity and assessment of the evolution in an eruption by considering the thermal output at the edifice.

Augustine Volcano is a small dome complex that forms an island near the mouth of Cook Inlet, Alaska (fig. 1). It erupted in January 2006 after a 20-year period of repose (Power and others, 2006). Seismic activity began increasing during May 2005, the first gas emissions began in September 2005, and steam plumes were first observed in satellite data on December 12, 2005. Between January 11 and 17, 2006, the volcano erupted explosively 13 times and then produced a continuous output of ash and gas from January 28 until February 2. After a hiatus, the volcano went into a two-week period of effusive eruption, which ended in mid-March. Located 280 km southeast of Anchorage International Airport, the volcano sits along the path of several local and international air traffic

[1]Alaska Volcano Observatory, Geophysical Institute, University of Alaska Fairbanks, 903 Koyukuk Drive, Fairbanks, AK 99775.

[2]Now at Scenarios Network for Alaska Planning, University of Alaska Geography Program, Fairbanks, AK 99775.

corridors (Power and others, 2006). To help prevent aircraft encounters with ash clouds, regional air traffic patterns were altered during the explosive phase of the eruption. Several nearby communities were affected by ashfall over this same period (Wallace and others, this volume).

Prior to 2006, there had been five known major historical eruptions (1883, 1935, 1963–64, 1976, 1986) of Augustine Volcano. Typically these events involved explosive eruptions followed by a period of lava effusion. Due to the relative repeatability of eruptions, the volcano was already well instrumented prior to the identification of precursory activity. As evidence increased that an eruption was likely to occur, the original instrumentation was greatly supplemented (Power and Lalla, this volume). The 2006 eruption of Augustine was the most intensely monitored eruption in AVO history, resulting in a multitude of datasets and providing an excellent opportunity to calibrate and validate satellite datasets. The range of activity displayed by the volcano provided a rich diversity of signals, with both explosive (of phreatic and magmatic origins) and effusive events occurring, and thus provided a robust test of AVO Remote Sensing (AVORS) group's operational capabilities.

This paper provides an overview of the observations made by AVORS using satellite data for all phases of the eruption. It highlights two areas of observation and analysis that are the primary capabilities of satellite-based volcano monitoring—thermal anomaly detection and ash cloud detection and tracking. On the basis of these datasets, we present discussions of the trends in the volcano's thermal output, discrepancies in the measurements of eruption cloud heights, and maps of the concentration and distribution of ash detected.

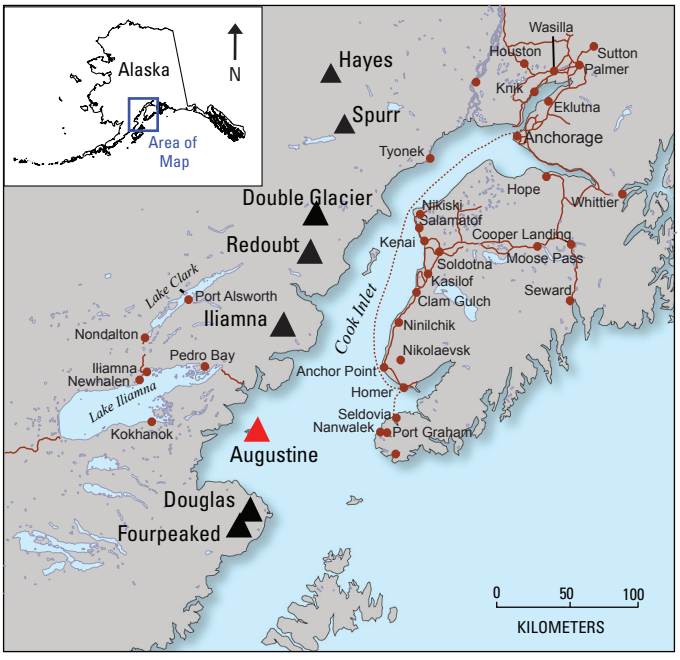

Figure 1. Map showing location of Augustine Volcano in Cook Inlet, Alaska. The area shown represents the Augustine sector that the Alaska Volcano Observatory remote sensing group creates from satellite data swaths to make large datasets more manageable during monitoring. Triangles indicate the location of volcanoes. Red lines show roads.

Background and Methodology

Satellite data provide quantitative information on volcanic clouds (Dean and others, 2002; Schneider and others, 2000) and elevated surface temperatures at volcanic edifices (Dehn and others, 2000; Harris and others, 1997, 2000). In recent years, new developments in satellite analysis have been implemented at AVO to harvest this information and make it available for operational monitoring purposes. These developments include systematic observation reporting using a dynamic database; Web-based imagery viewers; thermal anomaly detection and alarms; automated ash detection and compositing. Other tools, such as interfaces showing the detection of SO_2 using the Ozone Monitoring Instrument (OMI) and Atmospheric Infrared Sounder (AIRS) data have been developed through collaborations with other researchers. Satellite observations are supported by ground-based and airborne measurements (for example, use of a forward-looking infrared camera [FLIR]; Wessels and others, this volume); use of the Puff particle dispersion model (Searcy and others, 1998; Webley, this volume), ground-based aerosol samplers and LIDAR (Sasson and others, 2007; Webley and others, 2008), radar measurements (Schneider and others, 2006); webcam and pilot observations of activity. The operations of AVO combine all these measurements with those provided by seismology, geodesy and geology to create its best understanding of a volcanic event.

Satellite Datasets

The 2006 eruption of Augustine Volcano was the first operational test for many of the new remote sensing tools. They primarily analyze three satellite datasets: Advanced Very High Resolution Radiometer (AVHRR) data from the National Oceanic and Atmospheric Administration's (NOAA) Polar Orbiting Environmental Satellites (POES), Moderate Resolution Imaging Spectroradiometer (MODIS) data from the National Aeronautics and Space Administration's (NASA) Terra and Aqua satellites, and NOAA's Geostationary Operational Environmental Satellites (GOES) data. AVHRR and MODIS data are collected by receiving stations operated by the Geographic Information Network of Alaska (GINA) at the University of Alaska's Geophysical Institute. An additional AVHRR data feed is supplied by NOAA's Gilmore Creek satellite tracking station. GOES data are provided by the Naval Research Laboratory (NRL), Monterey Bay.

Data from these satellites/sensors are recorded in visible, mid-infrared, and thermal infrared wavelengths (table 1). AVHRR represents the "workhorse" for thermal anomaly and

Table 1. List of satellite data, wavelengths, and spatial and temporal resolution used to monitor volcanoes in Alaska.

[GOES, Geostationary Operational Environmental Satellites; NOAA, National Ocean and Atmospheric Administration; AVHRR, Advanced Very High Resolution Radiometer; MODIS, Moderate Resolution Imaging Spectroradiometer]

Satellite and Sensor[1]	Bands (B)	Wavelengths (μm)	Spatial Resolution (km)	Temporal Resolution (Repeat Coverage)
GOES Imager	1	0.52–0.72	8.0 at 60° N	0.5 hr
	4	10.5–11.5		
	5	11.5–12.5		
NOAA AVHRR (v3)	1	0.58–0.68	1.1 at nadir	Approx. every 1–2 hours at 60° N., due to large swath width and overlap
	2	0.73–1.00		
	3A (day)	1.58–1.64		
	3B (night)	3.55–3.93		
	4	10.3–11.3		
	5	11.5–12.5		
MODIS Terra/Aqua	28	7.175–7.475	1.0 at nadir	Approx. 2–4 passes per day
	29	8.4–8.7		
	31	10.78–11.28		
	32	11.77–12.27		

[1]All polar orbit except GOES (Geostationary).

ash detection. GOES is useful for tracking ash clouds because of its high temporal resolution. MODIS supplements the AVHRR thermal data and provides additional visible wavelength data allowing the creation of true color composites. Other data of opportunity (Landsat, Advanced Spaceborne Thermal Emission and Reflection Radiometer [ASTER]), which have high spatial resolution (<20 m/pixel) but infrequent repeat coverage (16+ days), can be used to corroborate observations made with AVHRR, MODIS, and GOES.

Detection Methodology

Dehn and others (2000) define a thermal anomaly (TA) as an unexpected increase in the radiant temperature value of a pixel in relation to its neighbors. For monitoring purposes, AVORS generally requires this difference (ΔT) to be >5°C to be of significance in any given dataset (AVHRR, MODIS, or GOES). However, in the early stages of activity at Augustine, observers were sensitive to smaller variations, especially when the anomalous pixels were located at the volcano's summit. Detection of thermal anomalies can be done either manually or using an automated algorithm. AVORS employs both methods, as there are a number of volcanological, environmental and technical explanations for TAs identified at a volcano, and not all are an indicator of volcanic activity. However, past history has shown that elevated radiant temperatures can often be a precursor to, or earlier indicators of, volcanic activity at Alaskan volcanoes, for example, Pavlof, 1996 (Roach and others, 2001), Okmok, 1997 (Patrick and others, 2003), Shishaldin, 1999 (Dehn and others, 2002), Cleveland, 2001 (Dean and others, 2004).

The 1996 eruption of Pavlof Volcano led to the creation of an algorithm that automatically processed images and identified thermal anomalies assessed to be of volcanic origin. This algorithm was successfully implemented during the 1997 eruption of Okmok and henceforth was known as the "Okmok Algorithm" (Dehn and others, 2000; Schneider and others, 2000; Dean and others, 2002). It has subsequently been updated (Okmok2) and augmented with a Web-based user interface that gives analysts access to a 15-year archive (1993+) of AVHRR images and Okmok Algorithm calculations for the North Pacific Region (fig. 2*A*). Additionally, if a thermal anomaly identified by the Okmok Algorithm meets certain criteria it generates warning emails and phone text messages that are sent to AVORS analysts. These alerts can also trigger a request for the acquisition of ASTER imagery at the volcano in question (Ramsey and Dehn, 2004).

Unfortunately it is difficult to create an algorithm that is 100 percent accurate in its identification of volcanic TAs, making manual checks an equally important part of regular monitoring activities. AVORS makes twice-daily manual checks of all acquisitions of AVHRR, MODIS, and GOES data and enters metrics for all identified thermal anomalies into a database using a Web-based interface. Reports that use a systematic template are then automatically generated and electronically distributed. The same database and electronic reports also include observations that are made of volcanic plumes and clouds.

The height and prediction of the movement of volcanic clouds are critical parameters required to assess their impact.

Satellite images offer a means to make these assessments, which would be difficult using only ground-based instruments and observations. Detection of these phenomena is complicated by the fact they might be composed of ash (of various size components), gas (of different species), or both. They might also assume different morphologies, related to atmospheric conditions, and whether they are a plume (generally used when the feature is still attached to the volcano) or a cloud (generally used when detached; that is, their volume is no longer being added to by the volcano). Although plumes will often have an elongated shape (due to regional wind effects) and higher ash density or steam content, volcanic clouds assume morphologies that can be hard to discriminate from surrounding meteoric clouds. Indeed all of these phenomena might not be seen on images if they are below higher altitude weather clouds.

As atmospheric winds carry volcanic clouds away from a volcano, diffusion and mixing cause them to spread, larger ash particles fall out, and their density is reduced. Thus an opaque cloud evolves into a translucent cloud. This evolution of volcanic clouds from opaque to translucent and the structure of the atmosphere both complicate and improve analyses (Schneider and others, 1995, 1999; Dean and others, 2004; Tupper and others, 2004). The identification of opaque versus translucent clouds requires the use of different bands in the satellite data. Opaque clouds appear as solid features, are colder than translucent clouds, and are usually visible in all bands. Translucent clouds by definition are less "solid" and often require a combination bands to be made visible.

Opaque clouds are needed to estimate height (table 2), where cloud-top temperatures measured from thermal IR band 4 (B4) satellite data are compared to atmosphere temperature profiles measured by sounders. This is referred to as the cloud temperature method. However, a major obstacle to the cloud temperature method is the tropopause, a position in the atmosphere where temperature does not decrease with height but stays about the same or, if above the tropopause, increases with height. An unambiguous height estimate can be derived only for clouds below the tropopause or larger umbrella clouds that reach into the stratosphere (Holasek and others, 1996; Tupper and others, 2007). For the 2006 Augustine eruption the lower tropopause boundary was at an altitude of approximately 8 km and upper boundary was at an altitude of approximately 16 km. Several of the 2006 Augustine eruptions were above the 8 km height.

Once a volcanic cloud becomes translucent valid cloud-top temperatures cannot be measured. However, a technique has been developed to detect translucent clouds that contain ash by subtracting long-wave thermal-infrared bands. This is referred to as the brightness temperature difference (BTD) or the split-window technique (Prata, 1989; Holasek and Rose, 1991). BTD values associated with volcanic ash have a negative signal between, 0 to −10 or lower, with the lowest value having the highest mass and presumably ash concentration for specific grain sizes (fig. 2*B*). Ash retrieval models have been developed to estimate ash particle size and total mass using BTD data (Wen and Rose, 1994; Schneider and others, 1999; Rose and Mayberry, 2000; Rose and others, 2001). Meteoric clouds can also exhibit negative BTD values, but the majority of these will not be more negative than −1.5. However, caution must be used when employing this technique, as volcanic clouds with ice-coated ash will not show a negative BTD signal (Prata 1989; Rose and others, 1995).

Ash Concentrations

One of the lessons learned from identifying and tracking the ash clouds produced by the Augustine eruptions was that it was easy to create a bottleneck in the flow of information being reported. This problem was caused by several factors: (1) six discrete eruptions occurred every few hours over a 20-hour period; (2) these events produced seven independently drifting ash clouds, visible in multiple datasets; (3) AVO reporting of ash clouds customarily involved text describing the position, direction of movement, and signal strength for each cloud on each image, a time consuming activity. In response to the bottleneck, a technique to produce composites of time-sequential BTD images was developed during post-eruption analysis. This method can act as a rapid visual summary of the previously cumbersome written descriptions.

There are three steps in the generation of the ash composites: (1) pixel values are extracted from selected images and compiled in a table, (2) BTD values are computed, and (3) values are displayed as an image. Three types of images are generated using the Most-Negative BTD values (Tupper and others, 2004), the Sum of BTD values, and Average BTD values. The Most-Negative image is generated such that the strongest BTD signal at each location is displayed and presumably includes the highest ash concentrations at that place. The Average image calculates average pixel values at each location and appears to identify signals that are related to the meteorological background, so it can be used to determine thresholds to differentiate weather from ash or other particulate signals. The Sum image is a simple summation of values at every location, but its usefulness is yet to be determined. Presently the Most-Negative images are automatically generated for each monitoring sector every 12 hours, with plans to implement updates in as near real-time as processing delays will allow. The images can viewed using a Web-based application, allowing multiple analysts to view the information simultaneously. These data have already proved to be a useful passive monitoring technique for small events at Cleveland (Alaska) and Bezymianny (Russia) volcanoes in 2007. However, as noted by Tupper and others (2004) some caution must be employed due to the failings of this technique for ice-coated ash.

Eruption Observations

The multitude of datasets collected during the eruption of Augustine permitted a detailed analysis of the events that

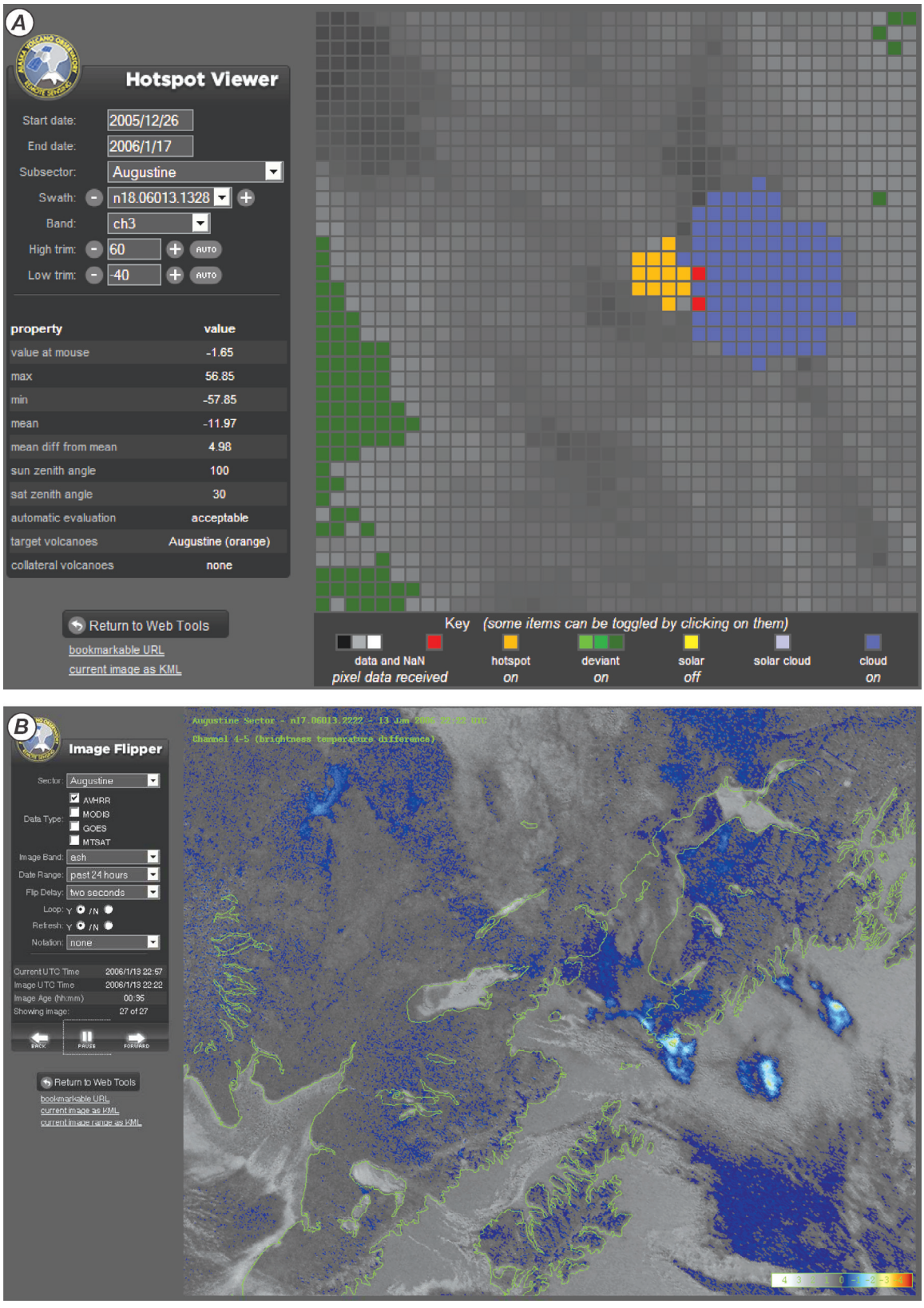

Figure 2. *A*, Web-based interface showing Okmok algorithm evaluation of an Advanced Very High Resolution Radiometer (AVHRR) image acquired at the start of Augustine Volcano's eruptive event 3 on January 13, 2006. *B*, Web-based interface showing a bright temperature difference evaluation of AVHRR bands 4 and 5 showing ash clouds from events 3, 4, and 5 at 1322 AKST (2222 UTC) on January 13, 2006.

Table 2. Augustine Volcano plume height observations.

[All satellite observations are based on AVHRR images unless noted. AKST, Alaska Standard Time; UTC, Coordinated Universal Time; NEXRAD, Next Generation Radar. See table 3 for dates of events]

Event	Satellite time (AKST/UTC)	Radar time (AKST/UTC)	Temperature based height (ft/km)	NEXRAD based height (ft/km)	Normalized difference wrt radar (%)	Comments
1	0456 1356	0449 1349	23,000 7.0	21,000 6.5	10	Tropopause (tropo) = 8.5 km., Plume < tropo.
2	0533 1433	0523 1423	28,900 8.8	33,500 10.2	−14	Tropo.= 8.5 km, Radar shows into tropo. Used 8.8 km for satellite.
3	0436 1336	0432 1332	29,500 9.0	33,500 10.2	−12	Tropo.= 8.5 km, Radar shows in tropo. Used 9 km for satellite.
4	1024 1924	0824 1749	NA	33,500 10.2	NA	Appears to be translucent cloud. Temperature values not valid.
5	1150 2050	1125 2025	29,500 9.0	34,500 10.5	−14	Tropo.= 9 km, Radar shows in tropo. Height 8 or 9 km for satellite.
6	1653 +0153	1642 +0142	32,000 10.0	34,000 10.5	−7	Tropo.= 9 km, Radar shows in tropo. Height 8 or 10 km for satellite.
7	1930 +0430	1930 +0430	36,000 11.0	34,500 10.5	4	Tropo.= 9 km, Radar shows in tropo. Height 7 or 11 km for satellite. GOES data.
8	0100 1000	0100 1000	23,000 7.0	20,000 6.1	15	Tropo.= 9 km, Radar < tropo. GOES data.
9	0838 1738	0801 1701	NA	45,000 13.7	NA	Tropo.= 9 km, Radar shows in tropo. Satellite temp. < meteoric cloud temp. suggests super cooling.
10	2042 +0542	2042 +0542	21,300 6.5	23,300 7.1	−9	Tropo. = 8 km, Radar shows < tropo.
11	NA	1140 +0840	NA	12,500 3.8	NA	No satellite data. Clouds translucent.
12	NA	0208 1108	NA	23,300 7.1	NA	No satellite data. Clouds translucent.
13	NA	0554 1654	NA	23,300 7.1	NA	Appears to be a translucent cloud.
14	NA	NA	NA	NA	NA	No satellite data.

occurred. The diversity of these datasets was further enriched by the range of activity displayed with explosive (of both phreatic and magmatic origins) and effusive events occurring. The evolution of the eruption was defined by four distinct phases, characterized by different styles of activity, and a hiatus (fig. 3; Coombs and others, this volume). The first phase was the precursory stage, which indicated increasing unrest at the volcano. Phase two saw the onset of explosive eruptions and culminated with a continuous eruption of material that defined phase three. This was followed by a hiatus during which the ash-cloud producing explosions stopped and the effusive activity that began sometime during phase two stalled. The fourth and final phase saw lava emplaced at the summit of the volcano.

The following sections describe the satellite observations for each phase of the eruption and give an overview of the events at the volcano. Other papers in this volume undertake a further exploration of these various aspects of the eruption using remote sensing techniques. McGee and others (this volume) describe the precursory and syn-eruption gas emissions at the volcano. Van Manen and others (this volume) combine satellite-derived thermal and seismic data to describe the activity beginning 10 days before the explosive phase. The distribution of tephra deposits produced during the eruption are defined by Wallace and others (this volume), whereas Webley and others (this volume) describe dispersion modeling of the plumes that produced these deposits. Ground-based imagery collected by time-lapse and infrared cameras is described in Sentman and others (this volume) and Paskievitch and others (this volume).

All times are given as Alaska Standard Time (AKST). In addition, times that relate to specific satellite images are also given in Universal Time (UTC) as the imagery UTC for its time/date identifier name. AKST is equal to UTC minus 9 hours.

Precursory Phase

The precursory phase began as an increase of micro-earthquakes beneath the volcano starting April 30, 2005 (Power and others, 2006). Initially occurring once or twice a day, the frequency steadily increased to 15 per day by mid-December (Jacobs and others, this volume). GPS measurements suggested pressurization of the volcano at sea level centered beneath the edifice (Cervelli and others, 2006). Starting in December small phreatic explosions were recorded by seismometers (McNutt and others, this volume), the largest of which occurred on the 10th, 12th and 15th. The December 12 event led to vigorous steaming and formation of a gas plume that was visible in AVHRR and MODIS data. Gas emissions started on December 12 at 1140 AKST (2040 UTC) and continued to at least 0442 AKST, December 13 (1342 UTC), although meteoric cloud cover prevented observations for the next 10 hours. The plumes were observed in visible and mid-infrared-band data. Most of the observed plumes were narrow and semi-translucent extending to 125 km or more, mostly to the south-east. No negative signal was detected in the BTD data, which combined visual observations by webcams on Augustine, suggested that there was little to no ash in these plumes. They were below 1,500 m altitude based on sounder data collected at 0000 UTC, December 6, 2005, at Kodiak. The best image showing this activity was recorded by the MODIS Aqua satellite at 1323 AKST (2223 UTC) (fig. 4). These events represented the first activity at Augustine that was visible in satellite data.

Explosive Phase

Generally cloudy conditions obscured views through December 2005 and early January 2006. On January 5, 2006, a break in the cloud cover allowed weak thermal anomalies (ΔT <3°C) to be detected at 2024 and 2119 AKST (0524 and 0619, January 6 UTC). Simultaneous webcam images collected at Homer showed clear views of a steaming edifice. Mostly cloudy weather returned and prevented further activity being seen in satellite images until 2245, January 10, AKST (0745 UTC, January 11) when a thermal anomaly (ΔT = 4.3°C) and a gas plume were detected. The plume was attached to the volcano indicating that material was still being emitted, and drifted to the southwest and west with the leading edge 74 km west of the summit of the volcano. It was only detected in band 3 data. No plume signal was detected in the longer TIR bands (B4 and B5) or in the split-window data, suggesting that little or no ash was in this emission.

January 11, 2006

Six hours later, two explosive eruptions occurred on at 0444 AKST (1344 UTC) and at 0512 AKST (1412 UTC) (table 3). Views of the edifice captured by AVHRR and MODIS in the hours after the eruptions showed a weak thermal anomaly located at the summit with low band 3 (B3) radiant temperatures (fig. 3). No thermal anomalies were observed immediately preceding the explosions, potentially suggesting that there was little or no fresh juvenile lava in the conduit

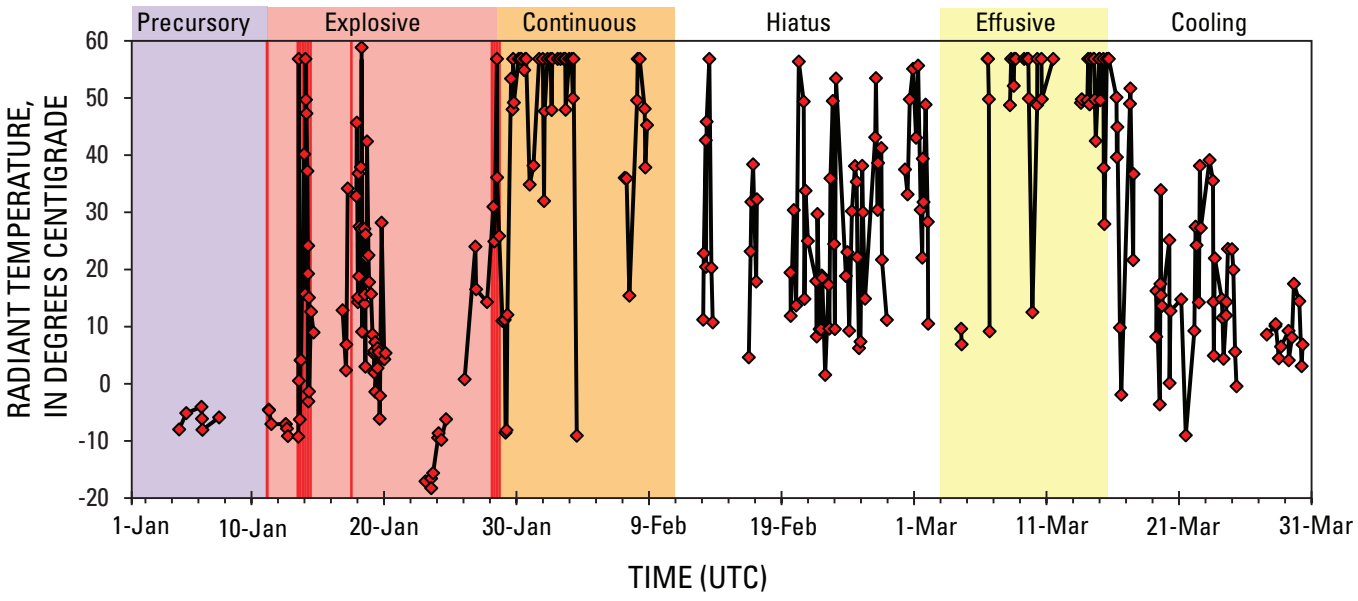

Figure 3. Plot of radiant temperatures of thermal anomalies seen at Augustine Volcano during the first 3 months of 2006 compared to eruption phases defined by geophysical measurements in Coombs and others (this volume). Vertical red lines represent explosive vents during the explosive phase.

that significantly contributed to the explosion. Analysis later confirmed that the ejected material was primarily older recycled debris (Wallace and others, this volume).

The material emitted by both of these eruptions was contained in a single opaque cloud although the curled tail of the second cloud may have been a remnant from the first eruption. The explosive eruptions were recorded on AVHRR satellite images within a few minutes of the start time of each event. The first image at 0448 AKST (1348 UTC) recorded the volcanic cloud 3 minutes after the explosive eruption ended (fig. 5*A*). This cloud was circular and directly over the volcano. The coldest volcanic cloud-top temperature was −46°C which corresponds to an altitude of approximately 7 km (23,000 ft) based on a dry atmosphere profile collected at Kodiak Island. Another image was recorded at 0525 AKST (1425 UTC), 10 minutes after the second eruption ended (fig. 5*B*). This cloud was also opaque and located over the volcano. It had a volcanic cloud-top temperature of −55°C, which corresponds to an altitude of approximately 8.5 km (28,000 ft) based on the same Kodiak atmospheric profile. Ground-based next generation radar (NEXRAD) estimates of volcanic cloud heights were similar for the first eruption with radar showing 6.5 km but were significantly different for the second with radar showing 10.5 km (Schneider and others, 2006). Wind directions suggested that the maximum cloud height was >8 km (~26,250 ft). The opaque cloud was observed in satellite images for 37 minutes, during which time the plume ascended 1.5 km (8,000 ft) at approximately 0.2 km/min (216 ft/min). On the basis of radar ascension rates were 0.108 km/min (355 ft/min).

GOES and AVHRR satellite passes recorded the movement, dispersion, and evolution of the plume. Images recorded

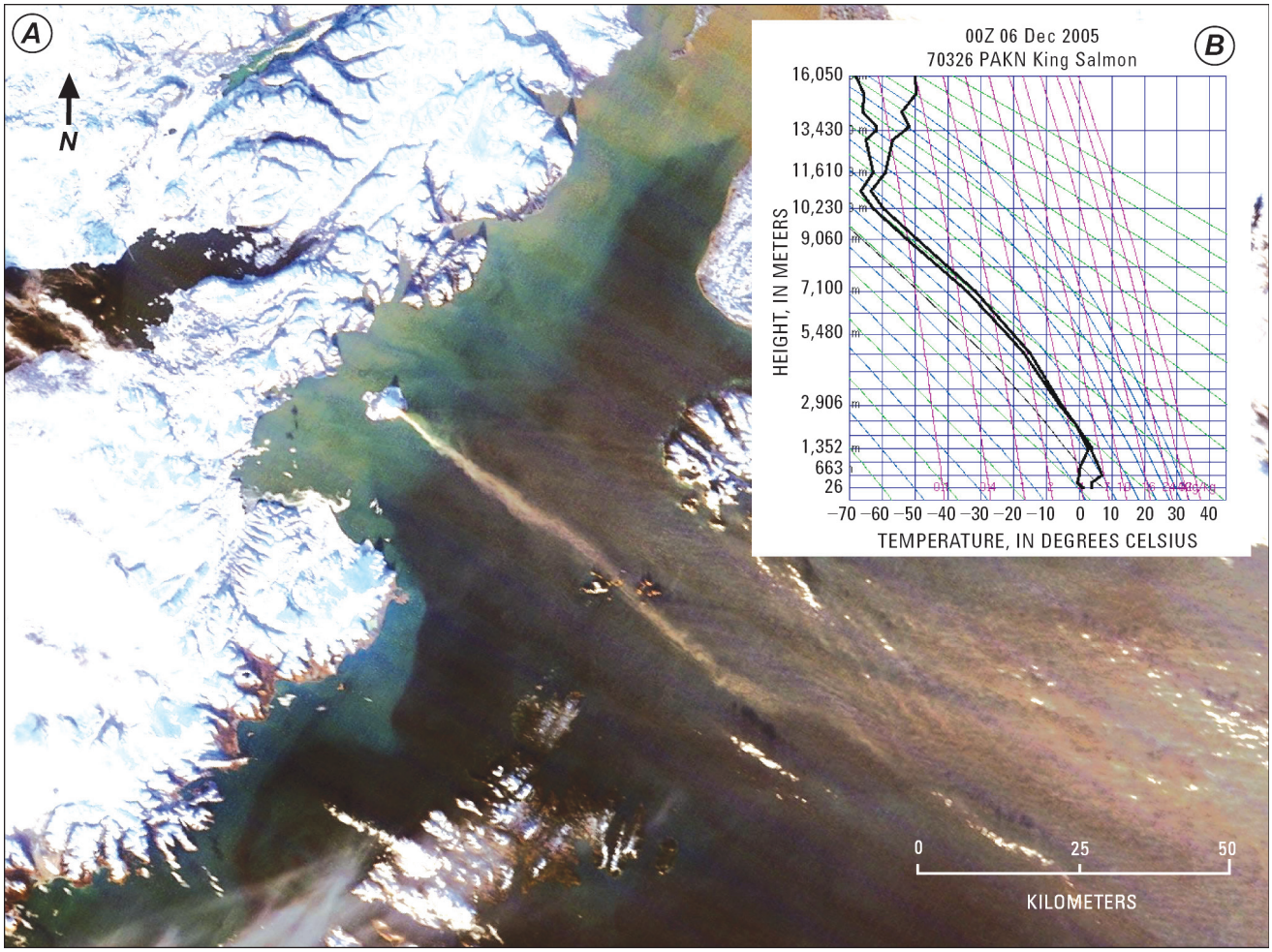

Figure 4. *A*, Moderate Resolution Imaging Spectroradiometer satellite true-color composite image showing a steam plume observed extending from Augustine Volcano for approximately 80 km (50 miles) to the southeast. There was no ash signal from the brightness temperature difference data indicating that this emission was most likely water vapor and SO_2. Image was acquired by the Terra satellite on 12 December 12, 2005 at 1216 AKST (2116 UTC) and processed by the Geographic Information Network of Alaska, University of Alaska Fairbanks. *B*, Regional radiosonde from the University of Wyoming's archive.

between 0530 and 0839 AKST (1430 to 1739 UTC) showed ash drifting to the northeast of the volcano, over Cook Inlet and the Alaska Peninsula. The opaque cloud began to disperse and become translucent at about 0530 AKST (1430 UTC), approximately 1 hour after the second explosion. These translucent clouds had BTD ash signals that ranged in value from −2.1 to −3.1, with the most negative values observed at 0730 AKST (1630 UTC; fig. 5). Data recorded after 0839 AKST (1739 UTC) had possible ash signals < −1, but these were not readily distinguishable from background noise. The cloud was mostly dispersed after 0930 AKST (1830 UTC). Generally, the strongest signals (< −3) were over water and within 20 km of the volcano. The majority of ash from these explosions probably fell into Cook Inlet. Very light ashfalls were reported approximately 100 km north-northwest at Lake Clark (Wallace and others, this volume) which is beyond the satellite-defined impact area. Most likely airborne ash in this region was at a concentration below the satellite detection threshold.

January 13–14, 2006

Six explosions (events 3 to 8) occurred on January 13 and 14 over a 25 hour period (fig. 6). Each explosion resulted in volcanic clouds that were tracked on 19 AVHRR satellite images, giving an average view of almost one image per hour. The first event for this period (event 3) occurred at 0424 AKST, January 13 (1324 UTC). An AVHRR image that was captured during the event (fig. 2*A*) showed an opaque cloud with a temperature of −54°C that reached an estimated altitude of 8.0 to 9.0 km based on sounder data collected at King Salmon. The cloud was still opaque when seen on a second image at 0456 AKST (1356 UTC), with a temperature of −52°C and was still at an altitude of approximately 8.0 to 9.5 km. NEXRAD radar reported a height of 34,000 ft (10.5 km). The cloud became translucent between images captured at 0637 and 0834 AKST (2 to 4 hours after the start of the eruption) with a BTD signal that weakened from −4.0 to −3.2 during this period. The volcanic cloud drifted east across Cook Inlet passing over the southern tip of the Kenai Peninsula. Ashfall was reported in the Homer, Seldovia, Port Graham, and Nanwalek areas between 0514 and 0850 AKST (Wallace and others, this volume). On the basis of satellite images, the ash cloud had moved east of Homer by 1024 AKST (1924 UTC) and by 1330 AKST (2230 UTC) the plume drifted over the coast near Seward, Alaska, and continued east across the Gulf of Alaska.

The second explosion (event 4) occurred at 0847 AKST (1747 UTC) and was recorded on an AVHRR image at 1024 AKST (1924 UTC). The image showed the cloud in transition from opaque to translucent and drifting east from the volcano. The cloud-top temperature of the opaque portion was −45°C, which suggested an altitude between 6.5 and 13.5 km based on sounder data collected at Kodiak. NEXRAD radar reported a height of 30,000 ft (9.1 km), and a pilot reported a height of 47,000 to 52,000 ft (14.3 to 15.8 km). The translucent portion of the cloud had a maximum BTD signal of −3.0 at the leading edge of the cloud that was approaching the Kenai Peninsula. This ash cloud passed over Seldovia and other towns at the southern tip of the Kenai Peninsula at 1130 AKST and then proceeded across the Gulf of Alaska. No ashfall was reported for this period from any towns in the area.

The third explosion (event 5) occurred at 1122 AKST (2022 UTC). Satellite images from 1130 to 1142 AKST (2030 to 2042 UTC) showed that the volcanic cloud was opaque with some translucent portions along its rim. The coldest cloud-top temperature of −54°C, observed at 1142 AKST (2042 UTC) translated to an altitude of 7.5 to 9.0 km based on sounder data collected at King Salmon. NEXRAD radar reported a height of 36,000 ft (11 km), and pilots reported a height of 52,000 ft (15.8 km). After 2042 UTC the cloud became more translucent as seen by an increase in cloud-top temperatures and increasing BTD signal strength. The ash cloud drifted east and passed over the lower Kenai Peninsula. It passed over towns in the vicinity of Seldovia from approximately 1322 to 1602 AKST and then continued across the Gulf of Alaska. No ashfall was reported for this period from any towns in the area.

The fourth explosion (event 6) occurred at 1640 AKST (0140 UTC, January 14). The first image recorded at 1645 AKST (0145 UTC, January 14) showed an opaque cloud with a translucent rim at the southern edge of Augustine Island that appeared to be still attached to the volcano. The minimum cloud-top temperature was −53°C, which corresponded to an altitude of 7.5 to 10.0 km based on the sounder at King Salmon. NEXRAD radar reported a height of 34,000 ft (10.4 km) and pilots reported a height of 30,000 to 35,000 ft (9.1 to 10.7 km). Images recorded around 1700 AKST (0200 UTC, 14 January) and later showed the cloud becoming translucent, as indicated by increasing cloud temperatures and increasing BTD signal strength. The most negative BTD signal of −4.0 was recorded at 1829 AKST (0329 UTC, 14 January). Unlike the previous events on this day, the ash cloud drifted to the south-east over Cook Inlet and the Gulf of Alaska. No ashfalls associated with this eruption were reported, and observations were unlikely because the cloud mostly drifted over the open ocean.

The fifth explosion (event 7) occurred at 1858 AKST (0358 UTC, January 14). GOES images recorded at 1900 AKST (0400 UTC, January 14) did not detect a volcanic cloud, probably due to its low spatial resolution at these latitudes, but the images at 1930 AKST (0430 UTC, January 14) and 2000 AKST (0500 UTC, January 14) showed an opaque cloud that was translucent along its periphery. The opaque cloud had a minimum temperature of −49°C on both of these images, which correlates to a height of 7 to 11 km based on the sounder at King Salmon. NEXRAD radar reported a height of 30,000 ft (9.1 km), and there were no pilot reports. The cloud became more translucent after 2000 AKST (0500 UTC, January 14), with the BTD-based ash signal reducing in strength over the next 3 hours. Time sequential GOES images

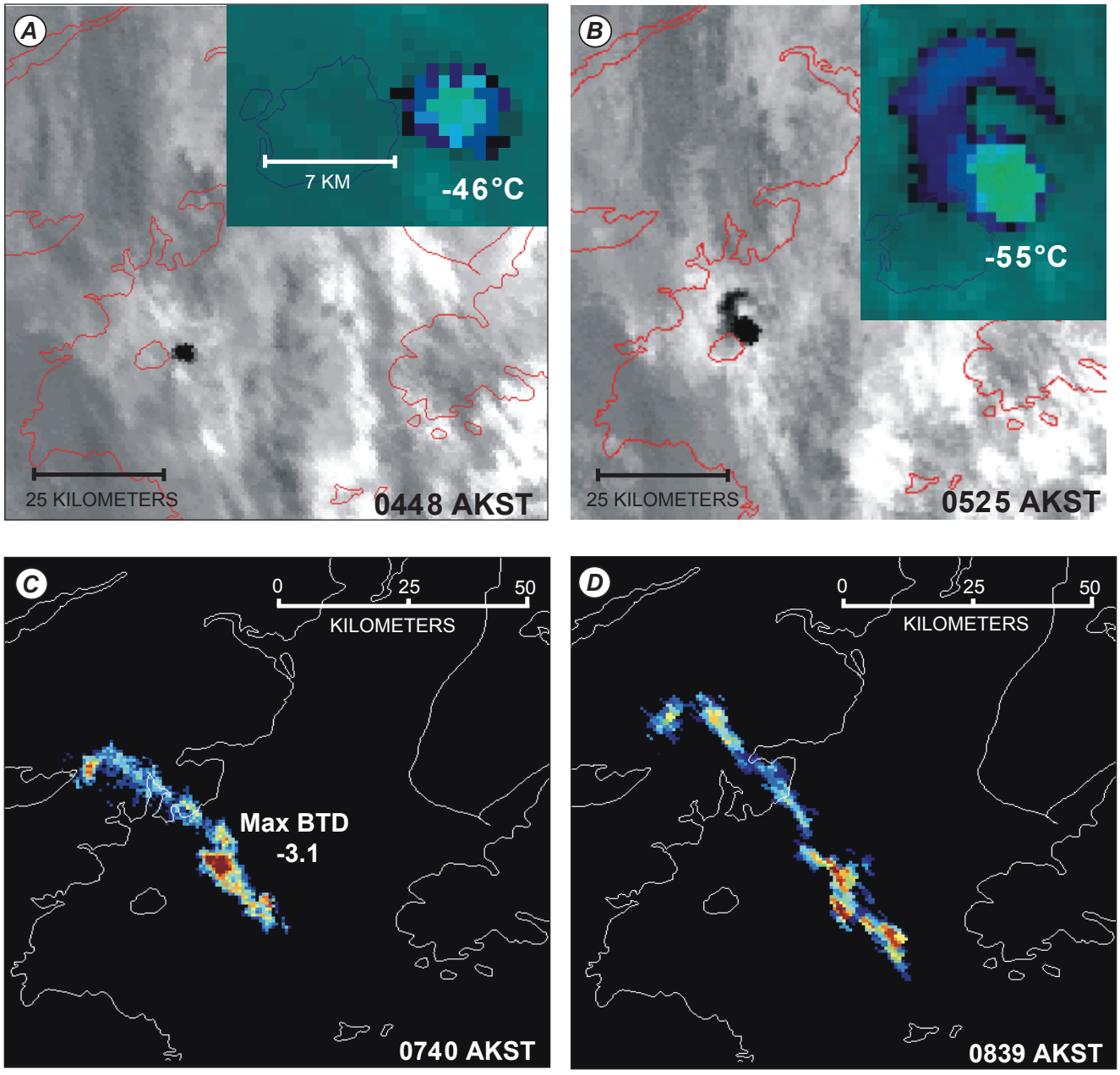

Figure 5. Advanced Very High Resolution Radiometer (AVHRR) satellite images of Augustine Volcano 2006 eruption event 1, the first explosive eruption. *A*, Band 4 thermal infrared image showing opaque cloud acquired at 0448 AKST (1348 UTC) on January 13, 2006. Insert shows enlarged view of the plume color-coded based on temperature. Coldest temperatures are indicated by light green pixels. *B*, Similar to *A*, acquired at 0525 AKST (1425 UTC). *C*, Brightness temperature difference (BTD) image showing the ash cloud drifting to the northeast over the Cook Inlet, acquired at 0740 AKST (1640 UTC). Most negative values of BTD are indicated by red pixels and indicate the highest concentration of ash. Moderate concentrations are shown by yellow and green pixels, with the blue pixels indicating the lowest concentrations of ash. *D*, Similar to *C*, acquired at 0839 AKST (1739 UTC).

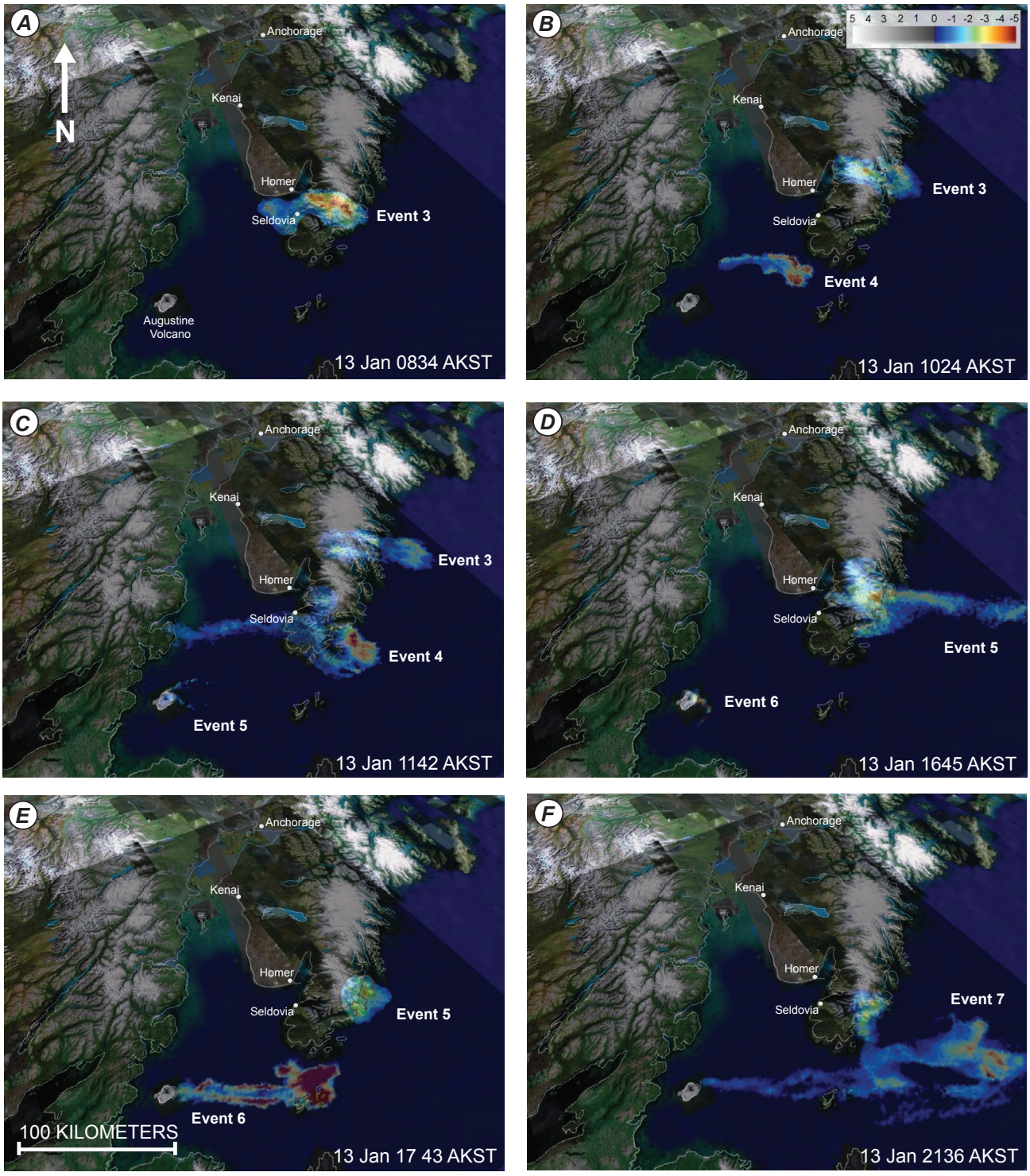

Figure 6. Advanced Very High Resolution Radiometer (AVHRR) data shown as brightness temperature difference images to detect ash clouds from the explosive events on January 13–14, 2006. The images are shown as overlays in Google Earth for geographic reference. Local time stamps are shown on images and equate to the following image UTC acquisition times: *A*, 1734, January 13; *B*, 1924, January 13; *C*, 2042, January 13, *D*, 0145, January 14; *E*, 0243, January 14; and *F*, 0636, January 14.

showed that the ash cloud drifted east over the lower Kenai Peninsula towns of Seldovia, Port Graham, and Nanwalek, but no ashfall was reported. Using just AVHRR data, it was difficult to distinguish event 7 ash clouds from previous ones in the general vicinity of the volcano. However, the high temporal resolution of time-sequential GOES data was sufficient to identify and track the movement of these ash clouds.

The sixth explosion (event 8) occurred on January 14 at 0014 AKST (0917 UTC). GOES satellite data recorded between 0030 and 200 AKST (0930 and 1100 UTC) showed an opaque cloud that became translucent as it dispersed. The opaque cloud had a minimum temperature of −50°C, which correlates to an altitude of 7.0 to 10.5 km. The translucent cloud had a maximum BTD signal strength of −3.2. The cloud moved east and north-east over the southern end of the Kenai Peninsula and the towns of Homer, Seldovia, Port Graham, and Nanwalek, then to the south-east across the Gulf of Alaska. No ashfalls were reported from this eruption.

Observations of thermal anomalies on January 13–14 were ambiguous due to the interaction of different effects. The maximum temperatures measured were a combined consequence of how long had passed since fresh, hot material was erupted and whether the volcanic cloud or steam at the volcano restricted views of the crater and surrounding deposits (fig. 3). In some images, solar reflection off the steam plumes also made the size of anomalies an uncertain parameter. In cases where images were collected with a clear view of the vent and/or fresh deposits around the edifice, AVHRR sensors reached their maximum calibration temperature (56.85°C) for band 3, and several pixels became saturated.

January 17, 2006

A further large explosion (event 9) occurred on January 17 at 0758 AKST (1658 UTC). GOES images recorded before the eruption showed a large weather cloud extending south-east and northwest from the volcano and approximately 200 miles long. The volcano erupted through this cloud. The GOES data recorded during and after the eruption did not show a distinct, coherent opaque volcanic cloud or definitive BTD ash signals that could be clearly distinguished from background weather signals. An AVHRR satellite pass at 0838 AKST (1738 UTC) did show a very distinct volcanic cloud in mid-infrared (B3) and thermal infrared (B4) wavelengths (fig. 7*B*). The B4 data showed minimum cloud-top temperatures of −56°C, which were colder than any height on the atmospheric temperature profiles collected at Kodiak. This suggested that the cloud was super-cooled, although this conclusion is tentative as the underlying meteoric cloud may have impacted the measured cloud temperature. The NEXRAD radar showed a maximum altitude of 45,000 ft (13.4 km), which indicated the ash cloud was well into the tropopause (Schneider and others, 2006).

Ashfall was reported from the Iliamna Lake and Lake Clark areas from 1200 to 1700 AKST (Wallace and others, this volume). A MODIS satellite image recorded on January 19, 2006 shows ash deposits on the snow-covered terrain west of Augustine Volcano beyond Iliamna Lake (fig. 7*A*). There was also a report of ashfall east of the volcano at Port Graham on the Kenai Peninsula. The AVHRR BTD data did not show the volcanic cloud extending to the east; however, Puff model predictions indicate that low level ash was predicted to pass over this area and thus the ash may have been below the detection limits of the satellite sensor (Webley and others, this volume). A similar situation occurred during the eruption of Cleveland Volcano in 2001, when a pilot reported the volcanic cloud well beyond the impacted area as defined by satellite data (Dean and others, 2004).

Similar to events on January 13–14, high radiant temperatures (>40°C) were only recorded in a few satellite passes following the explosion on January 17. The highest temperature measurement of 58.84°C was recorded at 2232 AKST (0732 UTC, January 18) in band 20b on Terra's MODIS sensor. Although values rapidly cooled from this peak, over the next 3 days elevated (above background) temperatures persisted (fig. 3). Poor weather conditions prevented observations January 20–23, but clear views on January 24 showed relatively weak thermal anomalies (ΔT = 10–15°C), with low radiant temperatures (<5°C).

Continuous Phase

Over the next 4 days the radiant temperatures increased rapidly, and activity moved into a phase that began with four more discrete explosions (events 10 to 14; table 3) that by 1430 AKST, (2330 UTC) January 28 transitioned into nearly continuous emission of gas and ash. Multiple ash clouds could be seen on most of the satellite data from this time until January 30 (fig. 8). The ash clouds drifted to the south on January 28 and 29 and then east after that time.

Eight minutes after the start of event 10, a satellite pass at 2042 AKST, January 27 (0542 UTC, January 28), showed an opaque cloud with a temperature of −45°C that correlated to estimated heights of 21,300, 31,200, or 47,600 ft (6.5, 9.5, or 14.5 km) based on atmospheric temperature profiles collected at King Salmon. Confusion in the true value was due to these heights being at or above the tropopause boundary. The maximum height recorded by radar was 34,500 ft (10.5 km), which puts the cloud top in the tropopause. The next satellite pass at 2115 AKST (0615 UTC, January 28) showed that the plume had become translucent with a BTD of −6.9 and was drifting south.

Events 11 and 12 were seen on four satellite passes between 2337 AKST, January 27 and 0745 AKST, January 28 (0837 to 1645 UTC, January 28). In the images translucent volcanic clouds with BTDs of −2.8 to −4.5, respectively, were seen drifting south over Kodiak Island. Event 13 was observed 34 minutes after the end of the eruption by a satellite pass at 819 AKST (1719 UTC) that showed a cloud which was part opaque and part translucent. The temperature of the opaque cloud was −45°C, which

corresponded to an estimated height between 19,700 and 32,800 ft (6.0 to 10.0 km) based on an atmospheric profile collected at Kodiak. The tropopause was at 19,700 ft (6.0 km). NEXRAD gave heights of 25,000 ft, and pilot reported heights suggested 35,000 ft. The translucent portion of the cloud had BTD values of −2.4, and as the cloud drifted south the BTD signal strengthened to a minimum of −7.4.

During the continuous phase, radiant temperatures at the summit anomaly remained consistently high (>45°C) until February 3, after which time cloudy weather prevented satellite observations. Thermal anomalies were observed in most images during this period with many images showing saturated pixels (fig. 9*A*), and most recording maximum AVHRR sensor values. The anomalies were large (10+ pixels) and varied in morphology. In some cases they were roughly circular and located around the summit, but in several images they were elongated along the flanks of the volcano. In a few instances the changes in size and morphology could be accounted for by solar reflection off steam and large satellite viewing angles, but in most cases these observations suggested pyroclastic flow activity on the volcano. This hypothesis was supported by webcam views (fig. 9*B*) and the color and morphology of deposits shown by a high resolution ASTER images (fig. 9*C*). Field studies later confirmed that there had been pyroclastic flow activity on the north and east flanks (Vallance and others, this volume).

Clear views on February 7 and 8 showed thermal anomalies with relatively high temperatures, but the values were decreasing in magnitude through the 8th. The thermal anomalies were much smaller than those observed a week before, and the greater size seen in some anomalies could be accounted for by radiation from, and solar reflection off, steam plumes. Poor weather prevented satellite views of the volcano from February 9–12, during which time the activity transitioned out of the continuous phase and average temperatures dropped to 20 to 30°C. The volcano now entered an eruptive hiatus that lasted almost a month. Ground-based observations, seismology, and geodesy all suggest that from February 10 to March 3 no new material was extruded from the volcano (Coombs and others, this volume).

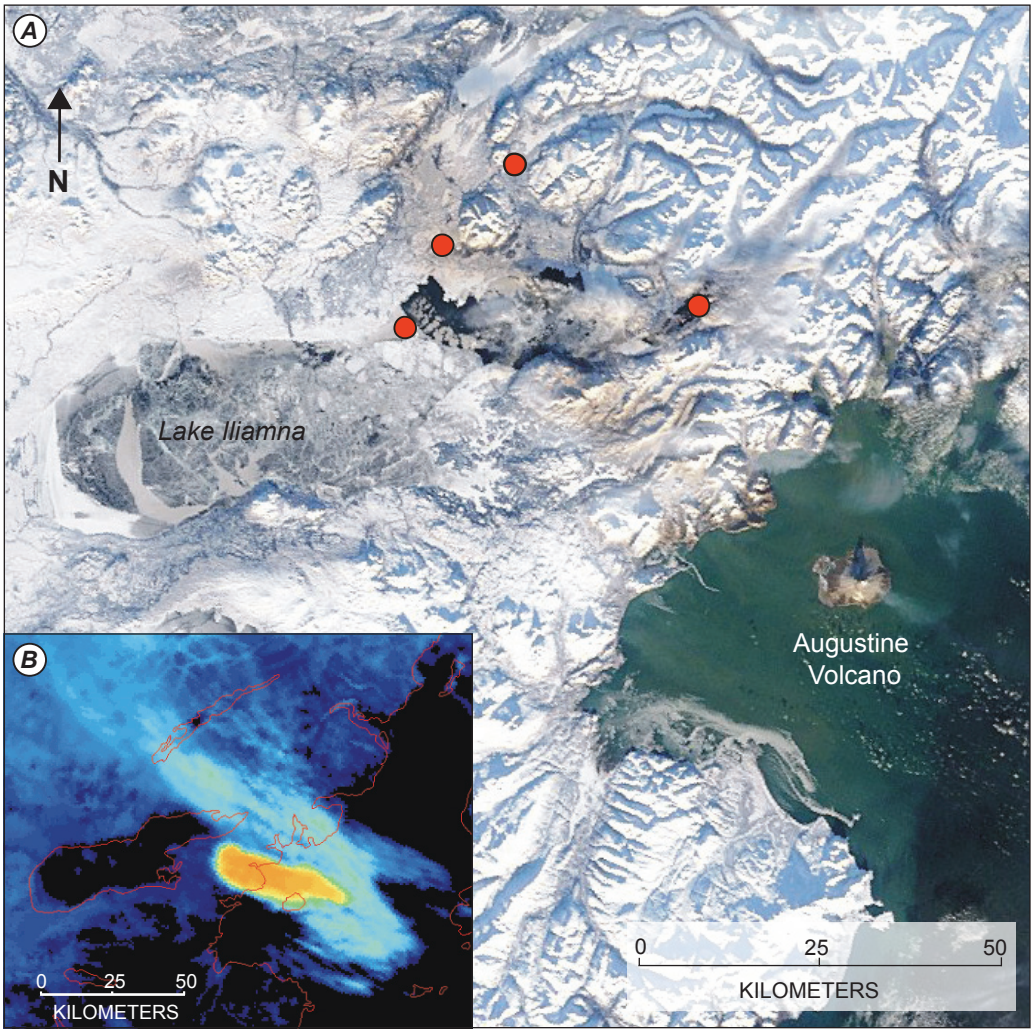

Figure 7. *A*, Moderate Resolution Imaging Spectroradiometer image showing ash fall from the eruption of Augustine Volcano on January 17, 2006. The ash cloud from the eruption drifted northwest from the volcano and dropped ash along a path that crossed the east end of Iliamna Lake, seen as brown tint in the snow. The red circles indicate (approximate) locations where light ash fall was reported or samples were collected. The image is a RGB color composite using visible bands 1, 4, and 3 acquired at 1240 AKST (2140 UTC) on January 19, 2006. *B*, Advanced Very High Resolution Radiometer band 4 view of the opaque ash cloud, acquired at 0838 AKST (1738 UTC) on January 17. Dense areas of ash are colored orange and yellow, with the distribution of finer ash shown in light blue.

Effusive Phase

During the 36 hours following the first explosions on January 11, several sequences of small, similar, regularly spaced volcano-tectonic earthquakes occurred, with rates as high as 3 to 4 per minute (Power and Lalla, this volume). Comparable sequences have been seen at other volcanoes, most notably Mount St. Helens (Dzurisin and others, 2005), in association with the emplacement of lava domes. During an over-flight on January 16, a new small dome was observed at the summit of Augustine Volcano. It was partly destroyed by the January 17 explosion, which blasted a 20 to 30 m crater in the dome. However, the lava dome continued to grow during January into early February and, after a period of hiatus, during March. The effusion of this final dome, and later two lava flows, defined the final phase of the activity (fig. 3).

The transition into the effusive phase was not observed by satellites due to cloudy weather that persisted from March 2–6. The radiant temperature values of two thermal anomalies that were observed on March 4 were greatly reduced by the cloud cover overhead. On the basis of seismic records, rockfalls increased on March 3 (Jacobs and McNutt, this volume), and on March 7 seismic activity once again became characterized by persistent, repetitive, and nearly identical earthquakes that increased in rate and size, forming a continuous signal by March 8 (Power and Lalla, this volume). Lava extrusion at the summit increased markedly in association with these signals (Power and others, 2006). As the volume of lava grew, two blocky lava flows moved down the volcano's north and north-east flanks (fig. 10). These deposits were highly unstable and generated multiple block-and-ash flows through regular collapses of volumes of fresh lava (Sentman and others, this volume; Vallance and others, this volume; Wessels and others, this volume)

The repetitive earthquakes began a slow decline in frequency after March 14 and disappeared by March 16 (Power and Lalla, this volume). A similar transition was seen in satellite data as thermal anomalies exhibited persistently high radiant temperatures (>45°C) until March 15–16, when temperatures began to decrease. Despite the cessation of effusive activity, frequent collapses of the dome and flows continued due to the unstable nature of the new material, leading to hotter material being exposed and contributing to the scatter seen in the overall cooling curve shown by the radiant temperatures (fig. 3).

Discussion

The eruption of Augustine Volcano provided an opportunity to robustly test monitoring methods and techniques recently developed by the AVORS group. The measurements these improvements made possible led to notable insights in three areas of interest: the patterns of thermal activity, ash cloud heights, and ash concentration mapping.

Table 3. Explosive events that occurred at Augustine Volcano during the explosive and continuous phase of its 2006 eruption.

[Time measurements are based on monitoring by seismic instruments. AKST, Alaska Standard Time; UTC, Coordinated Universal Time]

Event	Local time (AKST)	Time (UTC)	Duration (min: sec)
1	0444 11-Jan-06	1344 11-Jan-06	1:18
2	0512 11-Jan-06	1412 11-Jan-06	3:18
3	0424 13-Jan-06	1324 13-Jan-06	11:00
4	0847 13-Jan-06	1747 13-Jan-06	4:17
5	1122 13-Jan-06	2022 13-Jan-06	3:24
6	1640 13-Jan-06	0140 14-Jan-06	4:00
7	1858 13-Jan-06	0358 14-Jan-06	3:00
8	0014 14-Jan-06	0914 14-Jan-06	3:00
9	0758 17-Jan-06	1658 17-Jan-06	4:11
10	2024 27-Jan-06	0524 28-Jan-06	9:00
11	2337 27-Jan-06	0837 28-Jan-06	1:02
12	0204 28-Jan-06	1104 28-Jan-06	2:06
13	0742 28-Jan-06	1642 28-Jan-06	3:00
14	1430 28-Jan-06	2330 28-Jan-06	continuous

Patterns of Thermal Activity

Thermal anomalies for the Augustine eruption were defined by a combination of manual methods and automated detection using the Okmok II algorithm. Measurements using thermal-infrared channels on the GOES, AVHRR and MODIS satellite sensors are integrated values for areas of 1 km^2 and higher for each pixel (table 1). This limited spatial resolution limits the use of these datasets to describe the details of volcanic activity at Augustine. However, the high frequency of repeatability does allow trends to be seen. As described in the observations section these trends can be correlated to styles of activity, providing further supporting evidence for the definition of phases (fig. 2). More detailed descriptions of the activity and erupted products' thermal morphology require higher resolution thermal data (for example, ASTER), or use of ground-based thermal imaging (Sentman and others, this volume; Wessels and others, this volume). However, the satellite measurements can be used quantitatively to estimate erupted volumes and flux (Harris and others, 2007).

Ash Cloud Height Measurements

The 2006 Augustine eruption resulted in a large assortment of coincident observations that provided estimates or

measurements of volcanic cloud heights, more so than any previous Alaskan eruption. Typical measurement methods include cloud-top temperatures, wind shear, and pilot reports. Additionally, for the Augustine eruption a new technique, the ground-based NEXRAD radar, was available (Schneider and others, 2006). Each method can produce very different estimates of ash cloud heights and the recent Augustine eruptions were no exception (table 2).

Pilot observations provide on-site, instant estimates of the ash cloud heights but are also the least quantitative and generally give values much greater than other techniques. Measurements made by NEXRAD radar and the satellite cloud-top temperature also have the advantage of being collected at coincident times, allowing direct comparison. A normalized difference in percentage using the radar as control was calculated for each event using:

$$[(\text{Cloud-top Height Estimate} - \text{Radar Height Estimate}) / \text{Radar Height Estimate}] \times 100 \quad (1)$$

Radar is used as control because its radiometric response to the airborne particles is well known and the data were

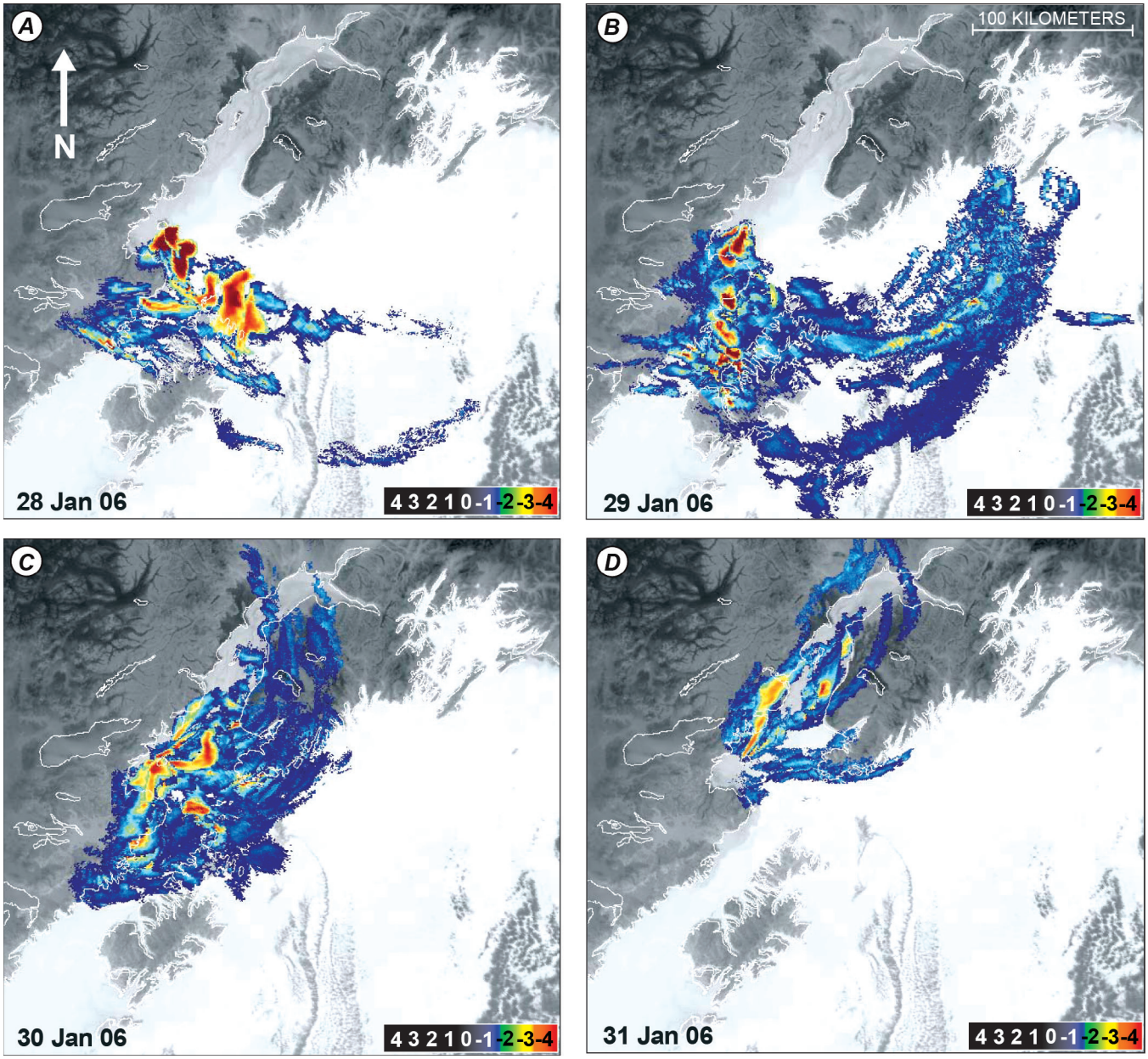

Figure 8. Composites of brightness temperature difference (BTD) data showing airborne ash distribution during the continuous phase of Augustine Volcano's 2006 eruption. Images show stacked data for one day's acquisitions on (*A*) January 28, (*B*) January 29, (*C*) January 30, and (*D*) January 31, 2006.

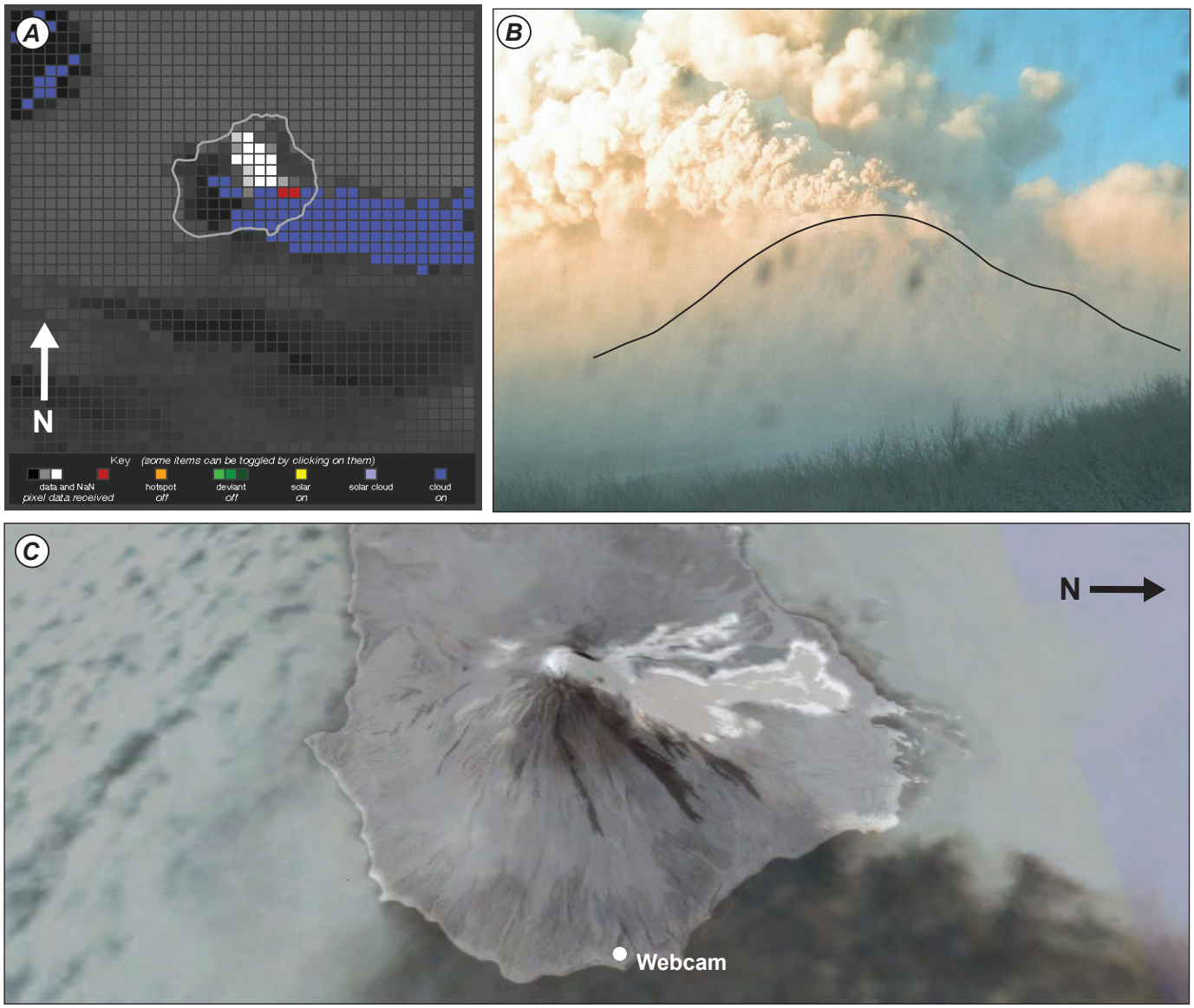

Figure 9. Views of ash clouds and pyroclastic flows generated during continuous phase of Augustine Volcano's 2006 eruption. *A*, Web viewer showing thermal anomaly (in white and shades of gray) in Advanced Very High Resolution Radiometer (AVHRR) image acquired 0829 AKST (1729 UTC) January 30. The white line defines Augustine Island. *B*, On island webcam view at 1016 AKST on January 29. The volcanic edifice is defined by a black line. *C*, Advanced Spaceborne Thermal Emission and Reflection Radiometer image acquired February 1, 2006, overlain on terrain in Google Earth. White areas show hot deposits. Views of hot deposits on east side of island are blocked by the ash cloud.

recorded consistently during the early stages of each eruption. Eight of the 14 events had sufficient satellite data to make this comparison. The comparison showed that all the cloud-temperature height estimates deviated by no more than 15 percent from the radar measurements (table 2).

However, there are some problems with the cloud-top temperature data. First, seven of the volcanic clouds were higher than 8.5 km, the approximate lower boundary for the tropopause, which means there are multiple heights that correlate to the cloud-top temperature. For these events it was assumed that the cloud ascended through the tropopause and reached natural buoyancy at the first height, which corresponded with the measured temperature. In reality, even if this was the case for the bulk of the cloud, there was likely some overshoot. Second, heights could not be estimated for six of the events due to missing data, because the cloud was translucent and valid temperatures could not be derived, or the cloud-top temperature was colder than the temperature of the atmosphere suggesting that this cloud was super-cooled and had not yet equilibrated to its surroundings (event 9).

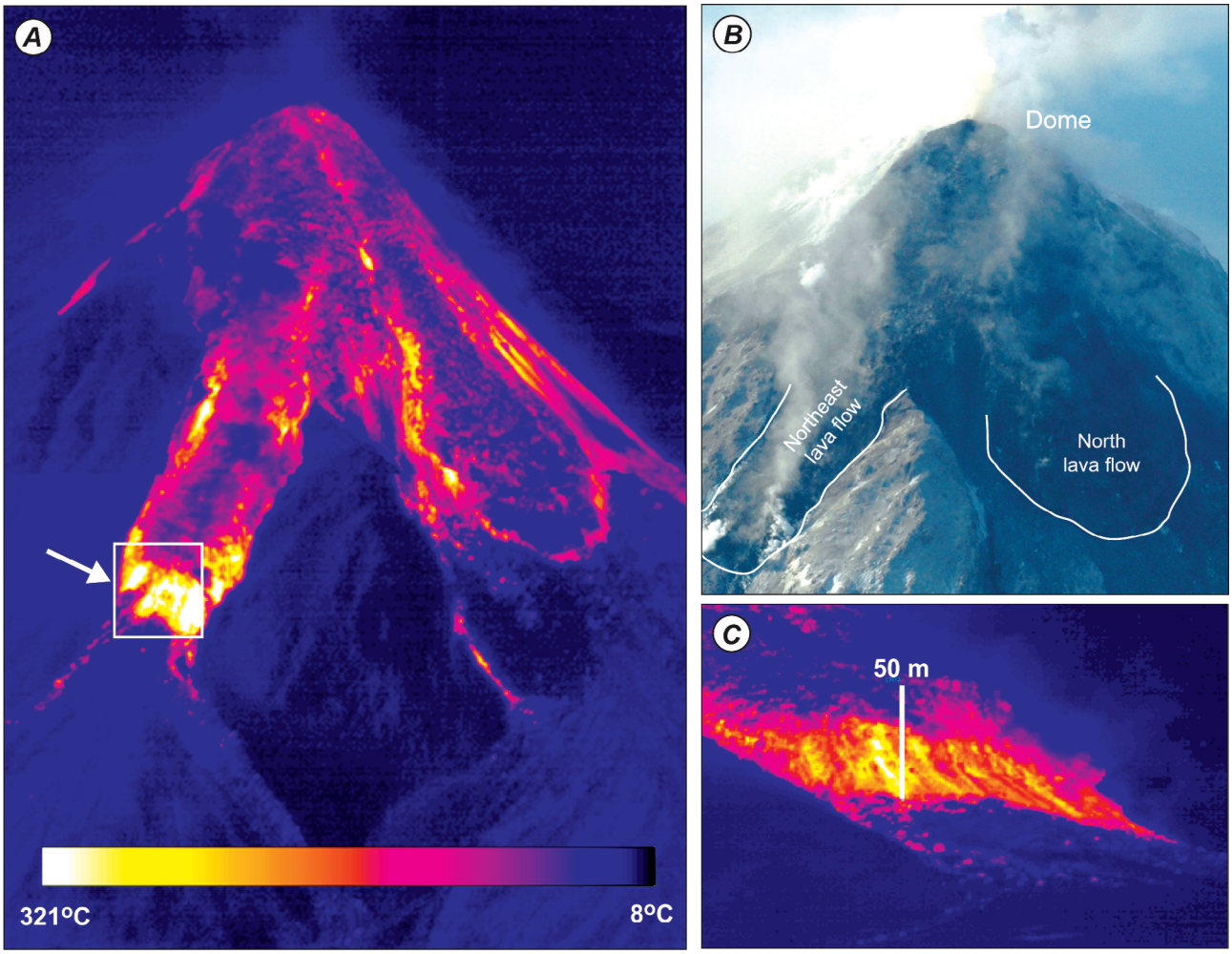

Figure 10. *A*, Forward looking infrared (FLIR) camera image showing Augustine Volcano summit lava dome and block flows on March 10, 2006 (FLIR images by Rick Wessels, AVO/USGS; Wessels and others, this volume). *B*, Photograph captured simultaneously with FLIR image (Photograph by Game McGimsey, AVO/USGS). *C*, Close-up of beveled front of the north-east lava flow. Location and angle of view shown by the white box and arrow in *A*.

Also, the comparisons for events 7 and 8 used GOES data, which has 8 km pixels, much larger than the 1.1 km pixels in AVHRR data. Thus GOES data are more likely to include a mixture of ground and cloud temperatures, resulting in a warmer reading and lower height estimate. Yet these still gave values to within the ±15 percent difference range.

Some of the variations in height estimates can be attributed to electromagnetic wavelengths used in detection. The NEXRAD method uses microwave energy and is sensitive to particle size and concentration. The cloud-top method uses thermal-infrared satellite data that detects smaller particles than radar does, and includes gaseous components (Schneider and others, 2006). Pilot reports are based on visual observations and are sensitive to water vapor and other gases appearing as the visible part of the cloud and are very qualitative (Simpson and others, 2001; Tupper and others, 2007). More quantitative visual measurements were made using oblique photography taken at the approximately the same time satellite images were acquired. These photos provided insight into the vertical structure of the eruption column and its relationship to the map view seen by satellites.

The eruption of event 6 provided an opportunity to compare and contrast these different techniques of cloud height measurement. Event 6 started at 1640 AKST on January 13. A satellite image at 1645 AKST (0145 UTC, January 14) showed a circular cloud over the volcano that was approximately 16 km across. A pilot reported a volcanic cloud up to 30,000 to 35,000 ft (9.1–10.7 km). The thermal-infrared image (fig. 11*A*) shows top-surface temperatures ranging from −15 to −30°C along its perimeter with much colder temperatures down to –53°C near the center, suggesting a height of 32,000 ft (10 km). Temperature differences in the cloud-top are usually

related to variations in height (Tupper and others, 2004), although if portions of the volcanic cloud are translucent, then the signal from the warm ground combines with the cold cloud and increases the detected temperature values. NEXRAD gave values of 34,000 ft (10.5 km).

A ground-based photograph at 1650 AKST (0150 UTC) showed a profile view of the same eruption column (fig.11*A*). The photograph was taken from Lake Clark, west of the volcano (fig. 11*B*). It shows a relatively flat cloud-top along the perimeter with a thin outer edge that thickens inward. Away from the perimeter the cloud's bottom extends below the ridge in the foreground and it is unclear whether it is still attached to the volcanic vent, making "plume" the more correct terminology. Seismic records indicated that the event had ended and additional material was no longer being erupted, implying it was at this point a volcanic cloud. Comparing the satellite image to the photograph shows that the warmer cloud temperatures approximately coincide with the thinner and translucent (few kilometers thick) perimeter. The central core is colder and most opaque. Towards the center of the cloud-top a high peak can be observed that most likely coincides with the coldest temperature. On the basis of measurements using the photograph, this cloud-top was estimated to be at an altitude of 9 km (29,500 ft), a value at the lower end of estimates by the other techniques.

Ash Composite and Concentration Maps

The ash composite technique is useful in delineating areas impacted by airborne ash. To show the area impacted by the Augustine eruptions, the most-negative ash composites were generated for January 11 (events 1–2), January 13 and 14 (events 3–8), January 28 through 31 (events 10–14 and continuous ash emission; fig. 8), and one image that combined images from all these dates (fig. 12). The eruption on January 17 was not included because it did not produce a cloud that could be identified by BTD techniques in satellite data. The combined image showed that the areas most heavily impacted based on airborne ash detected on satellite data are north, east, and south of the volcano.

These ash composites were used to identify and delineate concentrations based on ash signal strength. Ash signals less than −3 were assumed to include areas with the highest concentrations and were restricted to the area within approximately 80 km of the volcano (fig. 13). The ash signals with strengths 0 to −3 were assumed to include areas with moderate ash concentrations and extended as far as approximately 400 km from the volcano (fig. 13). Most of the ground-based ash samples, observations of ash deposits, and ash falling in the Cook Inlet area were located within the moderate ash concentration map unit. The majority of these samples and reports indicated light ash fall.

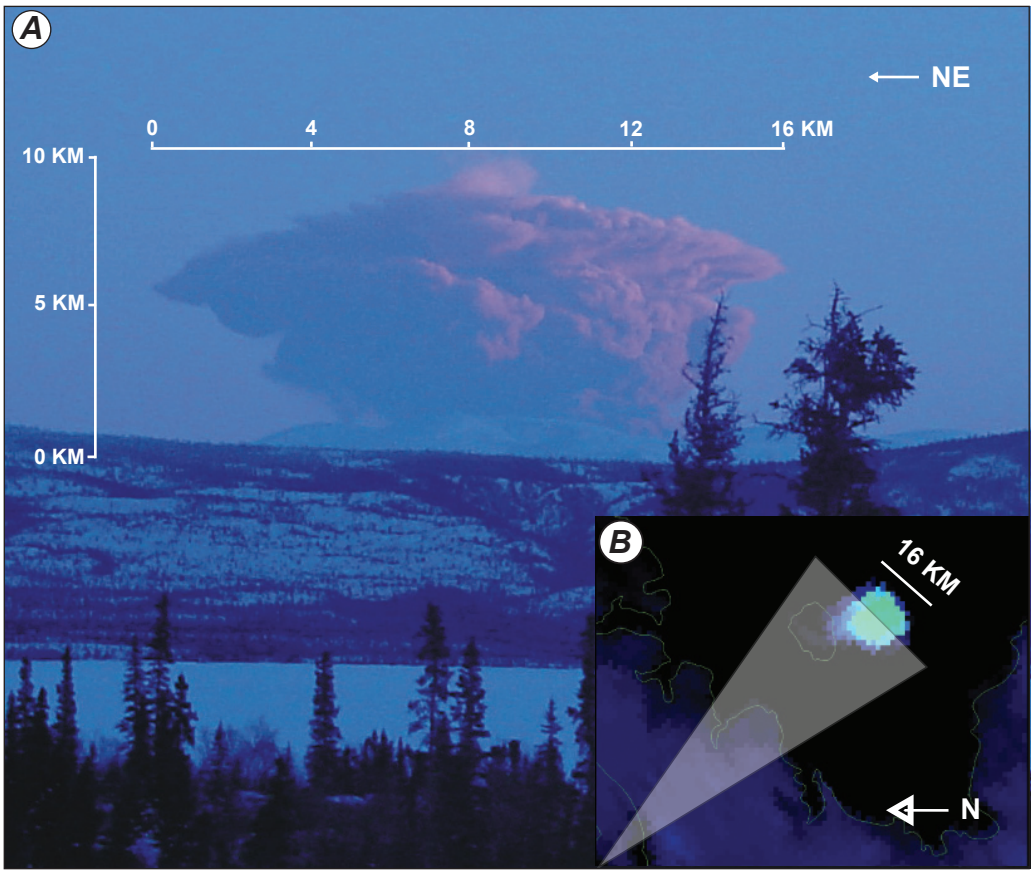

Figure 11. A comparison of an oblique photograph of an Augustine Volcano plume to a coincident satellite image. *A*, Oblique photograph of eruption cloud from event 6 on January 13, 2006 (Photograph by Leslie Beard). *B*, Advanced Very High Resolution Radiometer (AVHRR) band 4 image acquired at 1645 AKST, January 13, 2006 (0145 UTC, January 14).

The Puff dispersion model predicted the extent of ash beyond that observed on satellite data (Webley and others, this volume). These distal areas were north and east of the volcano and were considered to be the lowest concentrations (fig. 13). Measurements of airborne ash from ground-based LIDAR instruments at Fairbanks and Barrow (Sassen and others, 2007; Webley and others, 2008), aerosol samplers in Fairbanks and a snow sampler at Shasta, California (C. Cahill, written communication) validated the presence of the distal ash cloud. The Shasta ash was the most distant sample, at 1,800 miles (3,000 km) from the volcano. The distal portions of the plume presumably contained concentrations of ash below the detection limits of the satellite sensors and/or environmental conditions prevent detection by these sensors. It is likely that there were low airborne ash concentrations in these areas because no ash fall was reported by observers.

Conclusions

The 2006 eruption of Augustine Volcano provided an opportunity to test the robustness of several new tools that have been developed over the past few years by the AVORS group. It was also a catalyst for the development of new techniques and methodologies that have further complemented these primarily Web-based tools.

The thermal trends were observed at Augustine using satellite data in the 3 to 5 micron range. These data proved to be a good proxy for identifying the phases of eruption that were delineated using a range of geophysical measurements and visual observations. The success of the satellite data in defining the phases of eruption demonstrates the utility of remote sensing for monitoring Alaska's more remote but active volcanoes, such as Cleveland Volcano in the Aleutian Islands, which are not otherwise directly instrumented.

The multiple ash clouds erupted by Augustine allowed a comparison of multiple techniques that assessed the altitudes reached by these clouds. These methods included the use of satellite-based temperatures, ground-based radar, oblique photography, and pilot reports (PIREP). Instrument measurements proved to fairly consistent (table 2), but greater discrepancies occurred when comparisons were made to pilot's visual observations. These findings provide a cautionary tale for relying solely on one source for these data during monitoring operations.

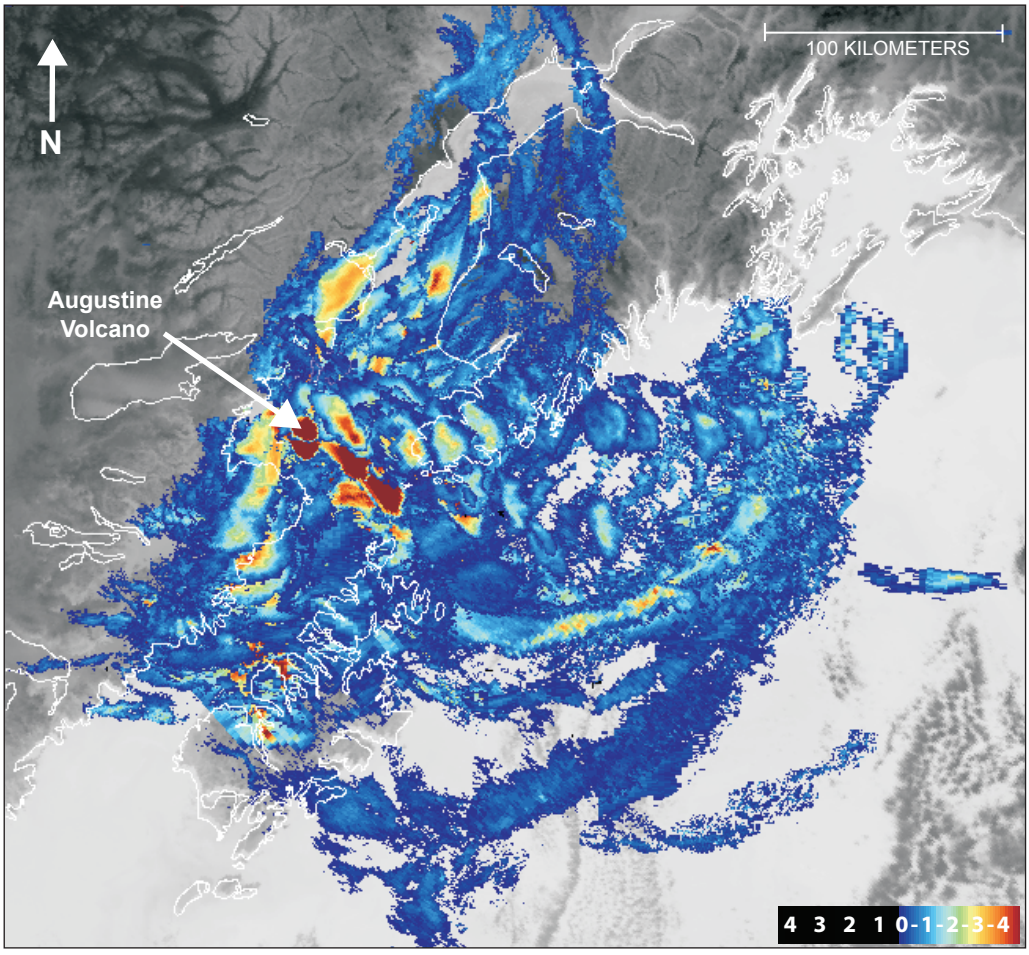

Figure 12. Brightness temperature difference (BTD) image showing combined airborne ash distributions from explosive Augustine Volcano eruptions. Image was created using Advanced Very High Resolution Radiometer (AVHRR) data showing the most negative ash composites for January 11 (events 1–2), January 13 and 14 (events 3–8), and January 28 through 31, 2006 (events 10–14 and continuous ash).

Airborne ash from the Augustine eruptions primarily impacted areas to the north, east, and south of the volcano, including Anchorage, Alaska's largest city, and towns on the Kenai and Alaska Peninsulas and Kodiak Island. Light ash fall was reported at many locations in the Cook Inlet region. Distal portions of the cloud drifted north over Fairbanks and Barrow, Alaska, and as far away as Mount Shasta, California. Various airlines cancelled multiple flights into the Ted Stevens International Airport, Anchorage, in response to this eruption.

A significant shortcoming of present hazard mitigation is the ability to detect or accurately predict the concentration of airborne ash. Quantitative ash concentrations are critical information to assess potential hazards to machinery (aircraft), transportation infrastructure, buildings and health (Blong, 1984; Horwell and Baxter, 2006). The U.S. military considers ash concentrations greater than 50 mg/m^3 dangerous to jet engines (Foreman, 1994). The concentration of ash that resulted in the failure of all four engines on the KLM 747 jet aircraft in Alaska in 1989 were estimated to be 2,000 mg/m^3 (Foreman, 1994), and ash concentrations based on those on the ground below the airspace of the encounter were estimated to be 500 g/m^2 with 75 percent of these particles smaller than 20 microns (Casadevall, 1994). The U.S. National Ambient Air Quality Standards (NAAQS) state that particles smaller than 10 microns are dangerous to human health, as they can enter and accumulate the respiratory system (U.S Environmental Protection Agency, 2007). Particles 2.5 microns and less are referred to as fine particles and can lodge deeply in the lungs. NAAQS, under the clean air act, requires particulate matter of 10 microns and smaller not to exceed 150 µg/m^3/24 hr, and particles 2.5 microns and smaller are limited to 35 µg/m^3/24 hr. These limits are based on values that protect public health, as well as damage to animals, crops, vegetation, and buildings.

The ash concentration map created using data from the Augustine eruption (fig. 13) is a prototype for the type of information that is required. One limitation of these data is

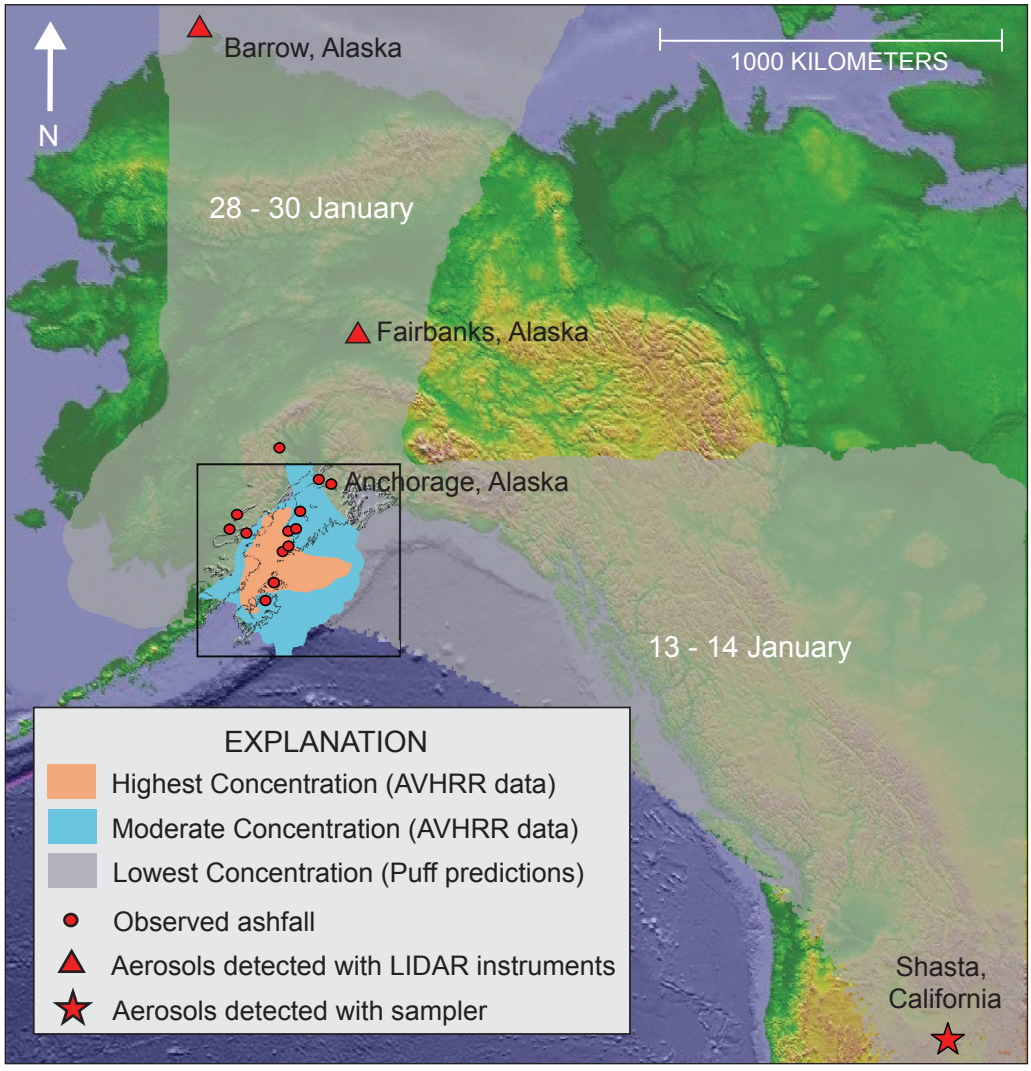

Figure 13. Map of relative ash concentrations from the eruptions of Augustine Volcano in January 2006. Based on combined airborne ash distributions (fig. 12), Puff model predictions (Webley and others, this volume), and ground-based observations and samples. AVHRR, Advanced Very High Resolution Radiometer; LIDAR, light detection and ranging.

that concentration assessments are based on relative quantities and do not give numerical values. The map units need to be calibrated so that they can be related to the hazard levels that can impact health and infrastructure, and to quantify the impact of a given event. This is an understanding that might prove crucial the next time Augustine or a similar volcano in the region erupts.

Acknowledgments

The authors would like to acknowledge the contributions of all the faculty, staff, and students that contributed to the AVORS's monitoring efforts during the eruption Augustine. In particular we thank Dave Schneider (AVO/U.S. Geological Survey) for his comments on cloud heights and William Ross (University of Alaska Fairbanks) and Joe Lovick (AVO/University of Alaska Fairbanks) for their contributions to the ash composite and distribution mapping.

References Cited

Blong, R.J., 1984, Volcanic Hazards—a sourcebook on the effects of eruptions: Sydney, Australia, Academic Press, 424 p.

Casadevall, T.J., 1994, The 1989–1990 eruption of Redoubt Volcano, Alaska—impacts on aircraft operations: Journal of Volcanology and Geothermal Research, v. 62,p. 301–316.

Cervelli, P.F., Fournier, T., Freymueller, J., and Power, J.A., 2006, Ground deformation associated with the precursory unrest and early phases of the January 2006 eruption of Augustine Volcano, Alaska: Geophysical Research Letters, v. 33, p. 5.

Coombs, M.L., Bull, K.F., Vallance, J.W, Schneider, D.J., Thoms, E.E., Wessels, R.L., and McGimsey, R.G., 2010, Timing, distribution, and volume of proximal products of the 2006 eruption of Augustine Volcano, *in* Power, J.A., Coombs, M.L., and Freymueller, J.T., eds., The 2006 eruption of Augustine Volcano, Alaska: U.S. Geological Survey Professional Paper 1769 (this volume).

Dean, K., Bowling, S.A., Shaw, G., and Tanaka, H., 1994, Satellite analyses of movement and characteristics of the Redoubt Volcano plume, January 8, 1990: Journal of Volcanology and Geothermal Research, v. 62, no. 1–4, p. 339–352.

Dean, K.G., Dehn, J., Engle, K., Izbekov, P., and Papp, K., 2002, Operational satellite monitoring of volcanoes at the Alaska Volcano Observatory, *in* Harris, A.J.H., Wooster, M., and Rothery, D.A., eds., Monitoring volcanic hotspots using thermal remote sensing: Advances in Environmental Monitoring and Modeling, v. 1, no. 3, p. 70–97.

Dean, K.G., Dehn, J., Papp, K.R., Smith, S., Izbekov, P., Peterson, R., Kearney, C., and Steffke, A., 2004, Integrated satellite observations of the 2001 eruption of Mt. Cleveland, Alaska: Journal of Volcanology and Geothermal Research, v. 135, no. 1–2, p. 51–73.

Dehn, J., Dean, K., and Engle, K., 2000, Thermal monitoring of North Pacific volcanoes from space: Geology, v. 28, no. 8, p. 755–758.

Dehn, J., Dean, K.G., Engle, K., and Izbekov, P., 2002, Thermal precursors in satellite images of the 1999 eruption of Shishaldin Volcano: Bulletin of Volcanology, v. 64, no. 8, p. 525–534.

Dzurisin, D., Vallance, J.W., Gerlach, T.M., Moran, S.C., and Malone, S.D., 2005, Mount St. Helens reawakens: EOS (American Geophysical Union Transactions), v. 86, no. 3, p. 25.

Foreman, P., 1994, Warning systems and pilot actions in ash and aviation safety, *in* Proceedings of the first international symposium on volcanic ash and aviation safety: U.S. Geological Survey Bulletin 2047, p. 163–168.

Harris, A.J.L., Blake, S., Rothery, D.A., and Stevens, N. F., 1997, A chronology of the 1991 to 1993 Mount Etna eruption using advanced very high resolution radiometer data—implications for real-time thermal volcano monitoring: Journal of Geophysical Research—Solid Earth, v. 102, no. B4, p. 7985–8003.

Harris, A.J.L., Dehn, J., Calvari, S., 2007, Lava effusion rate definition and measurement—a review: Bulletin of Volcanology, v. 70, p. 1–22.

Harris, A.J.L., Flynn, L.P., Dean, K., Pilger, E., Wooster, M. J., Okubo, C., Mouginis-Mark, P.J., Garbeil, H., Thornber, C., De la Cruz-Reyna, S., Rothery, D.A., and Wright, R., 2000, Real-time satellite monitoring of volcanic hot spots, *in* Mouginis-Mark, P.J., Crisp, J.A., and Fink, J.H., eds., remote sensing of active volcanism: Geophysical Monograph, American Geophysical Union, v. 116, p. 139–159.

Holasek, R.E., and Rose, W.I., 1991, Anatomy of 1986 Augustine volcano eruptions as recorded by multispectral image-processing of digital AVHRR weather-satellite data: Bulletin of Volcanology, v. 53, no. 6, p. 420–435.

Holasek, R.E., Self, S., and Woods, A.W., 1996, Satellite observations and interpretation of the 1991 Mount Pinatubo eruption plumes: Journal of Geophysical Research—Solid Earth, v. 101, no. B12, p. 27635–27665.

Horwell, C.J., and Baxter, P.J., 2006, The respiratory health hazards of volcanic ash—a review for volcanic risk mitigation: Bulletin of Volcanology, v. 69, p. 1–24.

Jacobs, K.M., and McNutt, S.R., 2010, Using seismic *b*-values to interpret seismicity rates and physical processes during the preeruptive earthquake swarm at Augustine Volcano 2005–2006, *in* Power, J.A., Coombs, M.L., and Freymueller, J.T., eds., The 2006 eruption of Augustine Volcano, Alaska: U.S. Geological Survey Professional Paper 1769 (this volume).

McGee, K.A., Doukas, M.P., McGimsey, R.G., Neal, C.A., and Wessels, R.L., 2010, Emission of SO_2, CO_2, and H_2S from Augustine Volcano, 2002–2008, *in* Power, J.A., Coombs, M.L., and Freymueller, J.T., eds., The 2006 eruption of Augustine Volcano, Alaska: U.S. Geological Survey Professional Paper 1769 (this volume).

McNutt, S.R., Tytgat, G., Estes, S.A., and Stihler, S.D., 2010, A parametric study of the January 2006 explosive eruptions of Augustine Volcano, using seismic, infrasonic, and lightning data, *in* Power, J.A., Coombs, M.L., and Freymueller, J.T., eds., The 2006 eruption of Augustine Volcano, Alaska: U.S. Geological Survey Professional Paper 1769 (this volume).

Miller, T.P., and Chouet, B.A., 1994, The 1989–1990 eruptions of Redoubt Volcano—an introduction: Journal of Volcanology and Geothermal Research, v. 62, p. 1–10.

Paskievitch, J., Read, C., and Parker, T., 2010, Remote telemetered and time-lapse cameras at Augustine Volcano, *in* Power, J.A., Coombs, M.L., and Freymueller, J.T., eds., The 2006 eruption of Augustine Volcano, Alaska: U.S. Geological Survey Professional Paper 1769 (this volume).

Patrick, M.R., Dehn, J., Papp, K.R., Lu, Z., Dean, K., Moxey, L., Izbekov, P., and Guritz, R., 2003, The 1997 eruption of Okmok Volcano, Alaska—a synthesis of remotely sensed imagery: Journal of Volcanology and Geothermal Research, v. 127, no. 1–2, p. 87–105.

Power, J.A., Nye, C.J., Coombs, M.L., Wessels, R.L., Cervelli, P.F., Dehn, J., Wallace, K.L., Freymueller, J.T., and Doukas, M.P., 2006, The reawakening of Alaska's Augustine Volcano: EOS (American Geophysical Union Transactions), v. 87, no. 37, p. 373.

Power, J.A., and Lalla, D.J., 2010, Seismic observations of Augustine Volcano, 1970–2007, *in* Power, J.A., Coombs, M.L., and Freymueller, J.T., eds., The 2006 eruption of Augustine Volcano, Alaska: U.S. Geological Survey Professional Paper 1769 (this volume).

Prata, A.J., 1989, Observations of volcanic ash clouds in the 10–12 um window using AVHRR/2 data: International Journal of Remote Sensing, v. 10, no. 4–5, p. 751–761.

Ramsey, M., and Dehn, J., 2004, Spaceborne observations of the 2000 Bezymianny, Kamchatka eruption—the integration of high-resolution ASTER data into near real-time monitoring using AVHRR: Journal of Volcanology and Geothermal Research, v. 135, no. 1–2, p. 127–146.

Roach, A.L., Benoit, J.P., Dean, K.G., and McNutt, S.R., 2001, The combined use of satellite and seismic monitoring during the 1996 eruption of Pavlof volcano, Alaska: Bulletin of Volcanology, v. 62, no. 6–7, p. 385–399.

Rose, W.I., Bluth, G.J.S., Schneider, D.J., Ernst, G.G.J., Riley, C.M., Henderson, L.J., and McGimsey, R. G., 2001, Observations of volcanic clouds in their first few days of atmospheric residence—the 1992 eruptions of Crater Peak, Mount Spurr volcano, Alaska: Journal of Geology, v. 109, no. 6, p. 677–694.

Rose, W.I., Delene, D.J., Schneider, D.J., Bluth, G.J.S., Krueger, A.J., Sprod, I., McKee, C., Davies, H.L. and Ernst, G.G.J., 1995, Ice in the 1994 Rabaul eruption cloud—implications for volcano hazard and atmospheric effects: Nature, v. 375, p. 477–479.

Rose, W.I., and Mayberry, G.C., 2000, Use of GOES thermal infrared imagery for eruption scale measurements, Soufriere Hills, Montserrat: Geophysical Research Letters, v. 27, no. 19, p. 3097–3100.

Sassen, K., Zhu, J., Webley, P., Dean, K., and Cobb, P., 2007, Volcanic ash plume identification using polarization lidar — Augustine eruption, Alaska: Geophysical Research Letters, L08803, v. 34, p. 1–4.

Schneider, D.J., Dean, K.G., Dehn, J., Miller, T.P., and Kirianov, V.Y., 2000, Monitoring and analyses of volcanic activity using remote sensing data at the Alaska Volcano Observatory; case study for Kamchatka, Russia, December 1997, *in* Mouginis-Mark, P.J., Crisp, J.A., and Fink, J.H., eds., Remote sensing of active volcanism: Geophysical Monograph, American Geophysical Union, v. 116, p. 65–85.

Schneider, D.J., Rose, W.I., and Kelley, L., 1995, Tracking of 1992 eruption clouds from Crater Peak vent of Mount Spurr Volcano, Alaska, using AVHRR, *in* Keith, T.E.C., ed., The 1992 eruptions of Crater Peak vent, Mount Spurr Volcano, Alaska: U.S. Geological Survey Bulletin 2139, p. 27–36.

Schneider, D.J., Rose, W.I., Coke, L.R., Bluth, G.J.S., Sprod, I.E., and Krueger, A.J., 1999, Early evolution of a stratospheric volcanic eruption cloud as observed with TOMS and AVHRR: Journal of Geophysical Research — Atmospheres, v. 104, no. D4, p. 4037–4050.

Schneider, D.J., Scott, C., Wood, J., Hall, T., 2006, NEXRAD weather radar observations of the 2006 Augustine Volcanic eruption clouds: Eos (American Geophysical Union Transactions), v. 87, no. 52, Fall Meet. Supplement, abstract V51C-1686.

Searcy, C., Dean, K., and Stringer, W., 1998, PUFF—a high-resolution volcanic ash tracking model: Journal of Volcanology and Geothermal Research, v. 80, no. 1–2, p. 1–16.

Sentman, D.D., McNutt, S.R., Stenbaek-Nielsen, H.C., Tytgat, G., and DeRoin, N., 2010, Imaging observations of thermal emissions from Augustine Volcano using a small astronomical camera, *in* Power, J.A., Coombs, M.L., and Freymueller, J.T., eds., The 2006 eruption of Augustine Volcano, Alaska: U.S. Geological Survey Professional Paper 1769 (this volume).

Simpson, J.J., Hufford G., Pieri D., and Berg J., 2001, Response to ‘‘Comments on ‘Failures in detecting volcanic ash from a satellite-based technique’’’: Remote Sensing of Environment, v. 78, p. 347–357.

Tupper, A., Carn, S., Davey, J., Kamada, Y., Potts, R., Prata, F., and Tokuno, M., 2004, An evaluation of volcanic cloud detection techniques during recent significant eruptions in the western “Ring of Fire”: Remote Sensing of Environment, v. 91, no. 1, p. 27–46.

Tupper A., Itikarai I., Richards M., Prata F., Carn S., Rosenfeld D., 2007, Facing the Challenges of the international airways volcano watch—The 2004/05 Eruptions of Manam, Papua New Guinea: Weather and Forecasting, v. 22, no. 1, p. 175–191.

U.S. Environmental Protection Agency, 2007, Technology Transfer Network, National Ambient Air Quality Standards (NAAQS): [http://www.epa.gov/ttn/naaqs/pm/pm10_index.html].

van Manen, S.M., Dehn, J., West, M.E., Blake, S., and Rothery, D.A., 2010, The 2006 eruption of Augustine volcano—Combined analyses of thermal satellite data and reduced displacement, *in* Power, J.A., Coombs, M.L., and Freymueller, J.T., eds., The 2006 eruption of Augustine Volcano, Alaska: U.S. Geological Survey Professional Paper 1769 (this volume).

Vallance, J.W., Bull, K.F., and Coombs, M.L., 2010, Pyroclastic flows, lahars, and mixed avalanches generated during the 2006 eruption of Augustine Volcano, *in* Power, J.A., Coombs, M.L., and Freymueller, J.T., eds., The 2006 eruption of Augustine Volcano, Alaska: U.S. Geological Survey Professional Paper 1769 (this volume).

Wallace, K.L., Neal, C.A., and McGimsey, R.G., 2010, Timing, distribution and character of tephra fall from the 2005–2006 eruption of Augustine Volcano, *in* Power, J.A., Coombs, M.L., and Freymueller, J.T., eds., The 2006 eruption of Augustine Volcano, Alaska: U.S. Geological Survey Professional Paper 1769 (this volume).

Webley, P.W., Dean, K.G., Collins, R., Fochesatto, J., Sassen, K., Atkinson, D., Cahill, C., and Prata, A.J., 2008, Validation of a volcanic ash dispersion model during late January/early February 2006 eruption of Mount Augustine Volcano: Bulletin of American Meteorological Society, v. 89, p. 1647–1658.

Webley, P.W., Dean, K.G., Dehn, J., Bailey, J.E., and Peterson, R., 2010, Volcanic-ash dispersion modeling of the 2006 eruption of Augustine Volcano using the Puff model, *in* Power, J.A., Coombs, M.L., and Freymueller, J.T., eds., The 2006 eruption of Augustine Volcano, Alaska: U.S. Geological Survey Professional Paper 1769 (this volume).

Wen, S., and Rose, W., 1994, Retrieval of sizes and total masses of particles in volcanic clouds using AVHRR bands 4 and 5: Journal of Geophysical Research — Atmospheres, v. 99, no. D3, p. 5421–5431.

Wessels, R.L., Coombs, M.L., Schneider, D.J., Dehn, J., and Ramsey, M.S., 2010, High-resolution satellite and airborne thermal infrared imaging of the 2006 eruption of Augustine Volcano, *in* Power, J.A., Coombs, M.L., and Freymueller, J.T., eds., The 2006 eruption of Augustine Volcano, Alaska: U.S. Geological Survey Professional Paper 1769 (this volume).

Appendix 1. Satellite Observations

Table 4. Satellite observations of gas emissions from Augustine Volcano on 12–13 December 2005.

[AKST, Alaska Standard Time; UTC, Coordinated Universal Time; AVHRR, Advanced Very High Resolution Radiometer; MODIS, Moderate Resolution Imaging Spectroradiometer]

Satellite sensor	Time, date (AKST)	Time, date (UTC)	Length (km)	Direction	Comments
AVHRR	1310, 12-Dec	2210, 12-Dec	>110	SE	Visible in B2 and B3, no B4m5 signal
MODIS	1323, 12-Dec	2223, 12-Dec	125	SE	Very distinct plume
AVHRR	1356, 12-Dec	2256, 12-Dec	85	SE	Very faint steam plume, faint B4m5 signal
AVHRR	1423, 12-Dec	2323, 12-Dec	120	SE	Faint steam plume, no B4m5
AVHRR	1452, 12-Dec	2352, 12-Dec	30	SE	Very faint steam plume, faint B4m5
AVHRR	1605, 12-Dec	0105, 13-Dec	NA	E	Mysterious cloud, defined by a few pixels
AVHRR	0442, 13-Dec	1342, 13-Dec	100	ENE	Very distinct plume, with some B4m5 signal

Table 5. Satellite observations of volcanic clouds on January 11, 2006.

[Height measurements based on cloud temperatures. AKST, Alaska Standard Time; UTC, Coordinated Universal Time; BTD, Brightness Temperature Difference; GOES, Geostationary Operational Environmental Satellites; AVHRR, Advanced Very High Resolution Radiometer]

Satellite sensor	Time, date (AKST)	Time, date (UTC)	Plume temp (°C)	Max. BTD signal	Plume height (km)
AVHRR	0448, 11-Jan	1348, 11-Jan	−46	NA	7
AVHRR	0525, 11-Jan	1425, 11-Jan	−55	NA	8.5
GOES	0530, 11-Jan	1430, 11-Jan	NA	−2.1	NA
GOES	0600, 11-Jan	1500, 11-Jan	NA	−1.7	NA
GOES	0630, 11-Jan	1530, 11-Jan	NA	−2.2	NA
AVHRR	0659, 11-Jan	1559, 11-Jan	NA	−2.7	NA
GOES	0730, 11-Jan	1630, 11-Jan	NA	−3.1	NA
AVHRR	0740, 11-Jan	1640, 11-Jan	NA	−1.8	NA
AVHRR	0839, 11-Jan	1739, 11-Jan	NA	−1.2	NA

Table 6. Satellite observations of volcanic clouds on January 13–14, 2006.

[Height measurements based on cloud temperatures. AKST, Alaska Standard Time; UTC, Coordinated Universal Time; BTD, Brightness Temperature Difference; GOES, Geostationary Operational Environmental Satellites; AVHRR, Advanced Very High Resolution Radiometer]

Satellite sensor	Time, date (AKST)	Time, date (UTC)	Plume temp. (°C)	Max. BTD signal	Plume height (km)
AVHRR	0428, 13-Jan	1328, 13-Jan	−54[1]	NA	8 to 9
AVHRR	0456, 13-Jan	1356, 13-Jan	−52[1]	NA	8, 9.5
AVHRR	0637, 13-Jan	1537, 13-Jan	NA	−4.0	NA
AVHRR	0655, 13-Jan	1555, 13-Jan	NA	−4.0	NA
AVHRR	0749, 13-Jan	1649, 13-Jan	NA	−3.4	NA
AVHRR	0834, 13-Jan	1734, 13-Jan	NA	−3.2	NA
AVHRR	1024, 13-Jan	1924, 13-Jan	−45[1]	−3.0	6.5, 13.5
GOES	1130, 13-Jan	2030, 13-Jan	−41	−2.1	NA
AVHRR	1142, 13-Jan	2042, 13-Jan	−54	NA	8 to 9
GOES	1200, 13-Jan	2100, 13-Jan	−46	−2.1	NA
AVHRR	1203, 13-Jan	2103, 13-Jan	−51	NA	7.5
GOES	1230, 13-Jan	2130, 13-Jan	−45	−2.3	NA
AVHRR	1246, 13-Jan	2146, 13-Jan	−49	−2.2	NA
GOES	1300, 13-Jan	2200, 13-Jan	−44	−3.3	NA
AVHRR	1322, 13-Jan	2222, 13-Jan	−45	−2.3	NA
AVHRR	1437, 13-Jan	2337, 13-Jan	NA	−1.5	NA
AVHRR	1645, 13-Jan	0145, 14-Jan	−53	NA	7.5, 10
GOES	1700, 13-Jan	0200, 14-Jan	−44	2.1	NA
GOES	1730, 13-Jan	0230, 14-Jan	−44	−2.5	NA
AVHRR	1743, 13-Jan	0243, 14-Jan	−49	−3.9	NA
GOES	1800, 13-Jan	0300, 14-Jan	−39	−3.0	NA
AVHRR	1829, 13-Jan	0329, 14-Jan	NA	−4.0	NA
GOES	1830, 13-Jan	0330, 14-Jan	−36	−3.4	NA
GOES	1930, 13-Jan	0430, 14-Jan	−49	−2.4	7, 11
GOES	2000, 13-Jan	0500, 14-Jan	−49	−3.9	7, 11
GOES	2030, 13-Jan	0530, 14-Jan	−46	−3.0	NA
GOES	2100, 13-Jan	0600, 14-Jan	−43	−3.3	NA
AVHRR	2136, 13-Jan	0636, 14-Jan	NA	−2.6	NA
AVHRR	2204, 13-Jan	0704, 14-Jan	NA	−2.9	NA
AVHRR	2316, 13-Jan	0816, 14-Jan	NA	−0.3	NA
GOES	0030, 14-Jan	0930, 14-Jan	−47	−3.2	7, 10.5
GOES	0100, 14-Jan	1000, 14-Jan	−50	−3.0	7, 10.5
GOES	0130, 14-Jan	1030, 14-Jan	−50	−2.3	7, 10.5
GOES	0200, 14-Jan	1100, 14-Jan	−47	−3.1	7, 10.5

[1]Measurement uncertain.

Table 7. Satellite observations of volcanic clouds on January 17, 2006.

[Height measurements based on cloud temperatures. AKST, Alaska Standard Time; UTC, Coordinated Universal Time; BTD, Brightness Temperature Difference; GOES, Geostationary Operational Environmental Satellites; AVHRR, Advanced Very High Resolution Radiometer; MODIS, Moderate Resolution Imaging Spectroradiometer]

Satellite sensor	Time, date (AKST)	Time, date (UTC)	Plume temp. (°C)	Max. BTD signal	Plume height (km)
GOES	0830, 17-Jan	1730, 17-Jan	−51	NA	7.5, 9.1, 11
AVHRR	0838, 17-Jan	1738, 17-Jan	−56	NA	NA
GOES	0900, 17-Jan	1800, 17-Jan	−50	−2.2[1]	7.3
GOES	0930, 17-Jan	1830, 17-Jan	−47	−1.6[1]	NA
GOES	1200, 17-Jan to 1800, 17-Jan	2100, 17-Jan to 0300, 18-Jan	NA	NA	NA
MODIS	1240, 19-Jan	2140, 19-Jan	NA	NA	Ash fall on ground

[1]Measurement uncertain.

Table 8. Satellite observations of volcanic clouds on January 28–29, 2006.

[Height measurements based on cloud temperatures. AKST, Alaska Standard Time; UTC, Coordinated Universal Time; BTD, Brightness Temperature Difference; AVHRR, Advanced Very High Resolution Radiometer]

Satellite sensor	Time, date (AKST)	Time, date (UTC)	Plume temp. (°C)	Max. BTD signal	Plume height (km)
AVHRR	2042, 27-Jan	0542, 28-Jan	−45	NA	6.5, 9.5, 14.5
AVHRR	2115, 27-Jan	0615, 28-Jan	NA	−6.9	NA
AVHRR	0332, 28 Jan	1232, 28 Jan	NA	−4.5	NA
AVHRR	0349, 28-Jan	1249, 28-Jan	NA	−2.8	NA
AVHRR	0516, 28 Jan	1416, 28 Jan	NA	−3.6	NA
AVHRR	0819, 28-Jan	1719, 28-Jan	−45[1]	−2.4	6, 6.5, 10
AVHRR	0917, 28-Jan	1817, 28-Jan	NA	−7.4	NA
AVHRR	1211, 28-Jan	2111, 28-Jan	NA	−3.7	NA
AVHRR	1334, 28-Jan	2234, 28-Jan	NA	−4.3	NA
AVHRR	1516, 28-Jan	0016, 29-Jan	NA	−7.5	NA
AVHRR	1911, 28-Jan	0411, 29-Jan	NA	−6.8	NA
AVHRR	0709, 29-Jan	0709, 29-Jan	NA	−3.0	NA

[1]Measurement uncertain.